Studies on Structural and Physical Properties of Zr Substituted $Na_{0.5}Bi_{0.5}TiO_3$ and $Na_{0.5}Bi_{0.5}TiO_3$-$BaTiO_3$ Solid Solution for Vibration Sensor Application

Gottuparthi Vasundhara

(MS12M1002)

A Dissertation Submitted to

Indian Institute of Technology Hyderabad

In Partial Fulfillment of the Requirements for
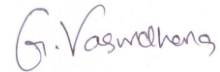
The Degree of Master of Technology

भारतीय प्रौद्योगिकी संस्थान हैदराबाद

Indian Institute of Technology Hyderabad

Department of Materials Science and Metallurgical Engineering

Indian Institute of Technology Hyderabad

June 2014

Declaration

I declare that this written submission represents my ideas in my own words, and where others' ideas or words have been included, I have adequately cited and referenced the original sources. I also declare that I have adhered to all principles of academic honesty and integrity and have not misrepresented or fabricated or falsified any idea/data/fact/source in my submission. I understand that any violation of the above will be a cause for disciplinary action by the Institute and can also evoke penal action from the sources that have thus not been properly cited, or from whom proper permission has not been taken when needed.

_____

(Signature)

Gottuparthi Vasundhara

(MS12M1002)

Approval Sheet

This thesis entitled "Studies on Structural and Physical Properties of Zr Substituted $Na_{0.5}Bi_{0.5}TiO_3$ and $Na_{0.5}Bi_{0.5}TiO_3$-$BaTiO_3$ Solid Solution for Vibration Sensor Application" by Gottuparthi Vasundhara is approved for the degree of Master of Technology from IIT Hyderabad.
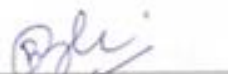
Dr. Atul Suresh Deshpande
Assistant Professor
Department of Materials Science and Metallurgical Engineering
Examiner

Dr. Bharat Bhooshan Panigrahi
Assistant Professor
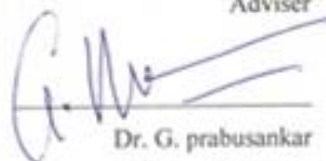Department of Materials Science and Metallurgical Engineering
Examiner

Dr. Ranjith Ramadurai
Assistant Professor
Department of Materials Science and Metallurgical Engineering
Adviser

Dr. G. prabusankar
Assistant Professor
Department of Chemistry
Chairman

iii

Acknowledgements

I am grateful towards my school teachers who introduced me to the basic science and make me to travel in this direction. I want to thank my mother for her constant love and blessings towards me and finally I am grateful to acknowledge my in laws especially my Father in law (**Mr. K.S.Rama Rao**), Mother in law (**Mrs. Samrajya Lakshmi**) and to my husband (**Mr. Udaya Bhaskar**) for their love and unlimited support to achieve my goal.

Dedicated to

My Family

&

My guide Dr. Ranjith Ramadurai

Abstract

In the present day modern technology scientists are more focused on lead free ferroelectric ceramics in understanding the fundamental issues, to improve the ferroelectric and piezoelectric properties of these materials. Among these lead free piezoelectric ceramics, sodium bismuth titanate $(Na_{0.5}Bi_{0.5})$ TiO_3 (NBT) in recent times has attracted much more due to its high ferroelectric and piezoelectric properties. It is well known that the structural and functional properties of materials can be tuned through the elemental substitution. In this regard, at present we have focused on tuning the piezoelectric properties of NBT ceramics via Zr substitution and NBT-BT solid solution. In order to synthesize both $(Na_{0.5}Bi_{0.5})$ $Ti_{1-x}Zr_xO_3$ and NBT-BT solid solutions conventional solid-state reaction route has been used. X-ray Diffraction, phonon mode measurements have been carried out to identify the structural and phase modifications. The sintered samples were electroded and poled to measure the dielectric and piezoelectric properties. The observation of relaxor features in Zr substituted NBT ceramics i.e. frequency dispersion in T_{max} along with diffused phase transition. In NBT-BT solid solution decrease in the depolarization temperature and T_{max} has been reported through dielectric studies. The electromechanical coupling coefficient of these materials has been measured using resonant and antiresonant method, which revealed the decrease in the coupling coefficient with substitutions. The piezoelectric strain coefficient was measured using Piezo-test meter for Zr substituted NBT and decrement in this value observed with Zr substitution. Finally these NBT ceramic pellets have been tested for the vibrational sensor applications.

Nomenclature

NBT - Sodium bismuth titanate ($Na_{0.5}Bi_{0.5}TiO_3$)

NBZT5 - Sodium bismuth zirconium titanate ($Na_{0.5}Bi_{0.5}Ti_{0.95}Zr_{0.05}O_3$)

NBZT10 - Sodium bismuth zirconium titanate ($Na_{0.5}Bi_{0.5}Ti_{0.9}Zr_{0.1}O_3$)

NBT-BT - Sodium bismuth titanate- Barium titanate solid solution ($(1-x)$ $Na_{0.5}Bi_{0.5}TiO_3-xBaTiO_3$)

NBT6BT - $0.94Na_{0.5}Bi_{0.5}TiO_3-0.06BaTiO_3$

NBT8BT - $0.92Na_{0.5}Bi_{0.5}TiO_3-0.08BaTiO_3$

ε - Dielectric constant or permittivity

ε'' - Dielectric loss

T_m or T_{max} - Temperature at maximum dielectric constant

γ - Diffusivity

T_c - Curie temperature

T_d - Depolarization temperature

XRD - X-ray diffraction

SEM - Scanning electron microscope

Contents

Chapter 1

Introduction

1.1 Dielectric materials:

The dielectric materials are electrically insulating and could be polarized by the application of electric field. In principle all the dielectrics are insulators, when an electric field is applied the center of positive and negative charges gets displaced which leads to net dipole moment. This separation of charge centers is called polarization [1]. Due to the polarizability of dielectric materials they are used in wide range of device applications staring from filters, data processors and storage etc. The energy storage is associated with the mechanism of charge separation under external electric field. The storage capacity varies from material to material; it depends on the intrinsic and extrinsic contributions of polarization.

Dielectric materials are classified into the two major types: non-ferroelectric materials and ferroelectric materials [2].

Non-Ferroelectric materials:

Non-ferroelectric materials get polarized when subjected to an external electric field. There are three major intrinsic mechanisms involved in the generation of electric polarization depending on the frequency of the applied electric field. The three primary mechanisms of polarization includes: electronic polarization, ionic polarization, orientational polarization (dipolar polarization) [2]. If the applied electric field induces the distortion of electron cloud around an atom then it is called as *electronic polarization*, which responds up to the frequency range of 10^{12} to 10^{15} Hz. The polarization generated due to the displacement of positive and negative ions with respect one another is called as *ionic polarization*, it follows the applied alternating field up to the frequency of 10^9 to 10^{12} Hz [2]. The alignment of dipoles in the direction of applied electric field is known as *orientational polarization or dipolar polarization*, it responds up to the frequency range of 10^6 to 10^9 Hz [Dipolar polarization presents in the materials possessing permanent dipoles] [2]. All these polarizations are due to bound charges within the system. Figure 1.1 shows the schematic representation of all these

polarization mechanisms. Apart from these polarizations the extrinsic contribution of polarization includes: space charge polarization, grains and grain boundary polarization [2].
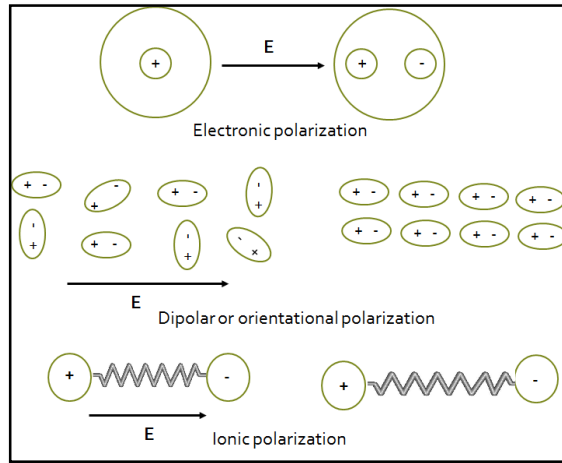
Fig 1.1: Electric polarization mechanisms

Ferroelectric Materials:

Ferroelectric effect was first observed by Valasek in 1921 in Rochelle salt. The word ferro is from Greek term *ferum* which means iron. This doesn't mean that it contains iron, the word ferroelectrics are used in analogy to ferromagnetism due to similarity in the characteristics. Ferroelectrics are the materials which exhibits spontaneous polarization and that can be reversible by the application of electric field [2]. The essential criterion of ferroelectric materials is the non-centro symmetric crystal structure which means lack of center of inversion. Most of the ferroelectric materials exhibit the perovskite crystal structure [General formula: ABO_3]
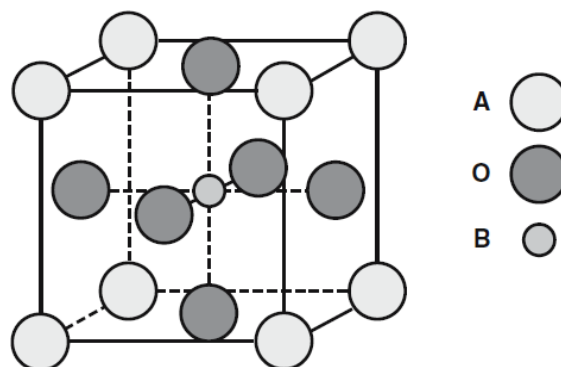
Fig 1.2: Schematic representation of a Perovskite Structure [5]

Features of Ferroelectricity:

Hysteresis behavior:

The nonlinear relation between polarization (P) and electric field (E) is called hysteresis behavior. Fig 1.3 shows the schematic of hysteresis loop of a conventional ferroelectric material. Initially the P varies linearly (OA region) with respect to applied field, because of insufficient field for the domain orientation. By increasing the field at a certain value the polarization gets saturated, which means most of the domains oriented in the direction field, it is called saturation polarization (BC region). Again by decreasing the field domains tried align in the original positions, whereas some of the domains could not orient in the original position. This leads to some remnant polarization (D) in the system even in the absence of external field. The field required to make the polarization zero is called coercive field (OR). The area of the hysteresis loop represents the energy dissipated in the specimen as heat during each cycle [2].
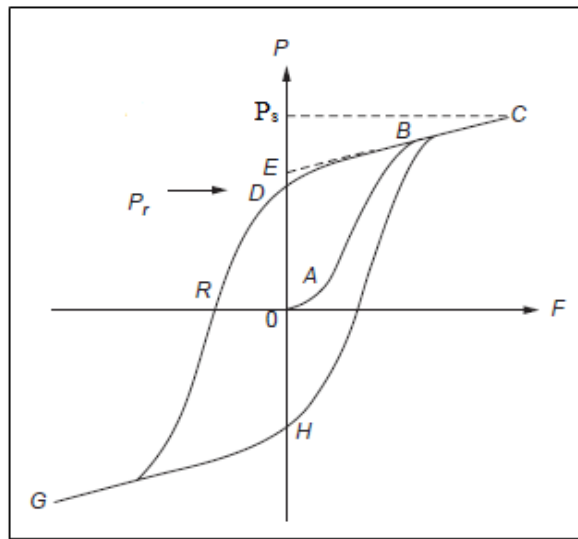
Fig 1.3: Hysteresis loop of ferroelectrics [2]

Structure criterion:

Non-centrosymmetric crystal structure is one of an essential criterion for a material to exhibit ferroelectric properties. Among the ferroelectric materials perovskites (ABO_3) structured materials are simplest, occupied major portion of ferroelectric materials. In the perovskites structure corner positions are occupied by the larger cations (A), body centered site is occupied by B cation, whereas all the face centered sites occupied by oxygen atoms.

3

Size of the A-site cation is larger compared to B, the interaction of A-O is more compared to B-O. So B-cation is free to move from its center position, this is called rattling of B cation, which is the origin of polarization in $BaTiO_3$ like systems [6]. The below figure (Fig 1.4) shows the origin of polarization in $BaTiO_3$.
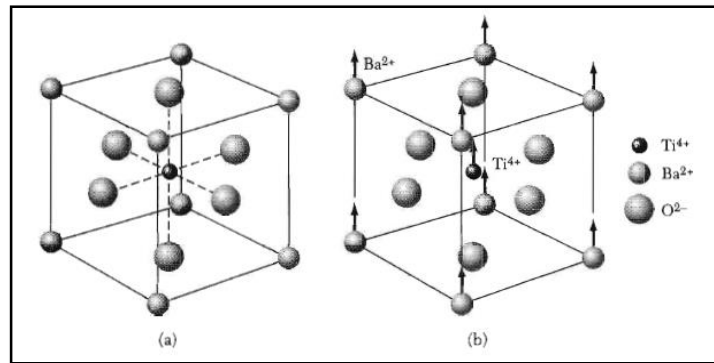
Fig 1.4: Origin of polarization in BaTiO₃ [6]

Phase transition:

The transition of a ferroelectric material from centro-symmetric state (paraelectric) to non-centro symmetric state at a particular temperature is called phase transition. The figure 1.5 shows the variation of a dielectric constant with temperature. In case of normal ferroelectrics the variation of dielectric constant is sharp when material undergoes transition from ferroelectric to paraelectric state. This transition involves structural changes and change in the spontaneous polarization [6]. The temperature at which phase transition occurs is called Curie temperature.
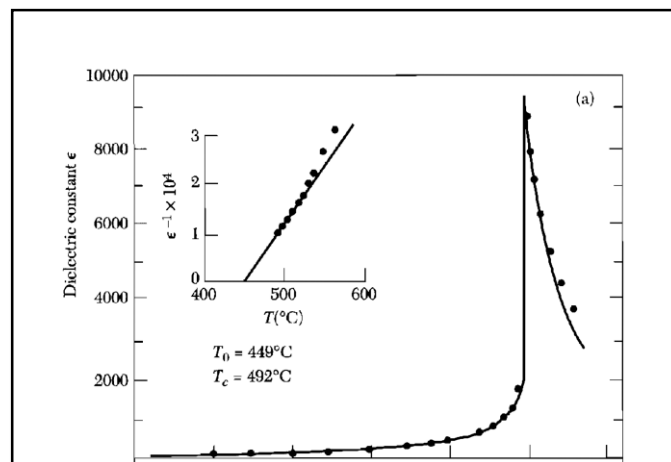
Fig 1.5: Phase transition in ferroelectrics [6]

4

1.2 Relaxor Ferroelectrics:

These are the special class of ferroelectrics, which has disorder at A or B site. The general formulae is $A_1A_2B_1B_2O_3$

here $A1 = Pb^{+2}$, Ba^{+2}, Sr^{+2}, Ca^{+2}, Na^{+1}; $A_2 = La^{2+}$, Bi^{3+}; $B_1 = Mg^{2+}$, Sc^{3+}, Zn^{4+}; $B_2 = Ti^{4+}$, Nb^{5+}

These relaxor ferroelectrics (RFE) are different from normal ferroelectrics in several aspects. The main properties of RFE are:

1. Due to presence of charge heterogeneity either in A-site or B-site cationic positions, relax or ferroelectric materials possess local cationic ordered and disordered regions. The ordered regions might be embedded in disordered regions and vice versa [3]. The ordered regions of relaxors are polar due to local structural distortion; these local ordered regions are also termed as polar nano regions (PNRs). The size of these polar nano regions in relaxors is typically in the order of 2-50nm.

2. Temperature dependence of permittivity in normal ferroelectrics follows the Curie-Weiss law i.e., $1/\varepsilon'$ vs T plot is follows the linear behavior after phase transition temperature (Curie temperature) as shown in the inset of figure. But relaxor-ferroelectrics exhibits strong deviation from Curie-Weiss law (non-linear $1/\varepsilon'$ vs T plot) due to the presence of interaction between polar nano regions even beyond temperature corresponds dielectric maxima (T_{max}) [4]. So the phase transition behavior of relaxor ferroelectric materials explained by modified Curie-Weiss law.

Modified Curie Weiss law: $(1/\varepsilon - 1/\varepsilon_m) = (T - T_m)^{\gamma} / C$ . . . . . . (1.1)

where, ε - Dielectric constant, ε_m - Maximum dielectric constant,

T_m - Temperature at ε_m

3. In relaxor ferroelectrics, ferroelectric to paraelectric transition is board i.e. over wide range of temperatures unlike normal ferroelectrics. Figure 1.6 shows the phase transition behavior of relaxor ferroelectric. The diffused phase transition in relaxors is due to variation in size of the ordered and disordered regions, as well as associated local compositional heterogeneity. Depending on the size of the clusters the temperature corresponds dielectric maxima (T_{max}) differs, so the phase transition is diffusive relaxors over wide range of temperatures. Additionally relaxors exhibits dielectric frequency dispersion below dielectric maxima, frequency dispersion in T_{max}. The shift in T_{max} towards high temperature in dielectric constant vs temperature curve with increasing frequency of the applied field (frequency dispersion in T_{max}) is

5

due to the increment of correlation strength between polar clusters as the measurement frequency increases [4].

(a)   (b)
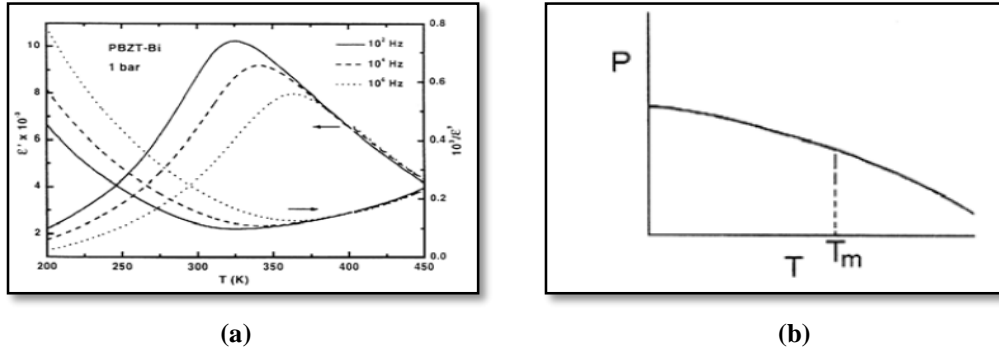
Fig 1.6 (a) Phase transition in relaxor ferroelectrics (b) Change in the polarization with temperature [4]

1.3 Piezoelectricity:

Piezoelectric effect was discovered by Jacques and Pierre Curie in 1888. The word piezo is derived from the Greek word **piezein** which means to squeeze or press. Piezoelectric effect is the capability of a material to generate the electric voltage by the application of mechanical stress. The essential requirement of a piezoelectric material is the crystal structure should be non-centrosymmetric. The major difference between ferroelectric and piezoelectric materials is: ferroelectrics exhibit reversible spontaneous polarization, whereas piezoelectrics (polar) exhibits non-reversible spontaneous polarization with no center of symmetry. Also non-polar piezoelectric materials do not exhibit any spontaneous polarization. Piezoelectric phenomena include both direct and indirect effects [2]. The generation of electric voltage under applied mechanical stress expressed as *direct piezoelectric effect*, whereas generation of mechanical strain (stress) by the application of electric field is called as *converse piezoelectric effect*.
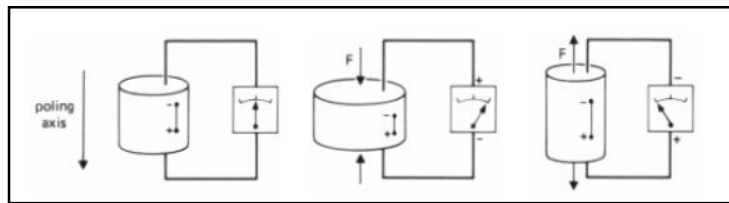
Fig 1.7: Piezoelectric effect phenomenon [7]

All ferroelectric materials are piezoelectric materials but all piezoelectric materials are not ferroelectrics. Piezoelectric materials with ferroelectricity exhibit reversible spontaneous

6

polarization whereas polar piezoelectrics without ferroelectricity exhibits irreversible spontaneous polarization.

Figures of merit:

Piezoelectric strain (charge) coefficient (d):

The Piezoelectric strain coefficient (d) is defined as the mechanical strain (x) induced in a piezoelectric material by the applied electric field along the specific direction or the amount of charge developed relative to the applied stress along the specific direction [8].

$$x = d\ \Delta E\ldots\ldots\ldots\ldots\ldots\ldots\ldots\ldots\ldots\ (1.2)$$

Piezoelectric properties are anisotropic in nature, so depending on the applied electric field direction the mechanical component will be different along different orientational direction. These directional properties are specified by using subscripts, which defines the direction and orientation. The more general form of strain coefficient is d_{ij}, where i is the applied field direction and j is the generated strain (or stress) direction. The Piezoelectric strain coefficients are d_{33}, d_{31} and d_{15}. The unit of piezoelectric strain coefficient is pm/V (or pC/N).

Electromechanical coupling factor (k^2):

Electromechanical coupling factor is the direct way to measure the energy conversion ability of a piezoelectric material to convert electrical energy to mechanical energy and vice versa. In other words coupling constant is a measure of efficiency of a piezoelectric material to convert one form of energy to another form [8].

$$k^2 = \text{Output electrical energy/ Input mechanical energy} \quad \text{(or)}$$

$$k^2 = \text{Output mechanical energy / Input electrical energy}\ldots\ldots\ldots(1.3)$$

The total input energy could not be converted into output energy, so the coupling factor (k) is always less than unity. Typical values of k are: 0.1 for quartz, 0.4 for Barium Titanate, 0.7 for Lead Zirconate Titanate (PZT) and 0.9 for Rochelle salt.

Chapter 2

Literature Review

2.1 Lead free Piezo ceramics ($Na_{0.5}Bi_{0.5}TiO_3$ (NBT)):

Lead based material are well known for their excellent piezoelectric properties and are widely using in various applications (marine, transducers, sonars and paints) and these materials are ruling the medical, electronic industry and structural health monitoring of civil structures. But considering the toxicity of lead and its compounds, which are emitted by the electronic waste, is hazardous to health and environment. So these materials are restricted from the ROHS (Restriction of hazardous substances), legislation passed by European Union [7].

So in recent years there has been a continuous drive in search of efficient lead free piezoelectric materials. In those lead free materials Bismuth based materials occupied a significant place due to its similarities with lead. Among all these Bi-based materials NBT is the most promising material with good piezoelectric properties due to the similarities in electronic configuration of lead and bismuth as in PZT lead leads to the polarization due to the distortion of stereo chemical $6s^2$ lore pair which is similar in NBT through Bi^{3+} ion. NBT was first reported by smolensky *et al.* in 1960. NBT phase transition behavior and crystal structure is still a controversial research topic. NBT has rhombohedral crystal structure at room temperature and shows phase transition with increasing temperature as Rhombohedral (*R3C*) to Tetragonal (*p4bm*) at 320 °C and Tetragonal to Cubic (*pm3m*) at 540 – 520 °C [9].

In general NBT is synthesized by solid state route and hydrothermal process depending upon the application. Barick *et al.* Prepared the NBT ceramic by solid state route at 1100 °C with 4 hrs. Because of this high sintering temperature there is a chance of Bi volatility which creates the oxygen vacancies in the system [9]. So to decrease the sintering temperature M.V. Raman *et al.* used microwave sintering method with 950 °C as sintering temperature. In both methods single phase sodium bismuth titanate is formed and by microwave sintering method improved the morphology and physical properties i.e. increase in the dielectric constant compared to solid state route was observed [10].

8

The dielectric properties of NBT are still an argument due to its diffused phase transition and without frequency dispersion in the T_{max} (the temperature corresponding to dielectric maximum). Fig. 2.1 shows the dielectric constant vs temperature at different frequencies. It was observed that dielectric constant (ε_r) increases with decreasing frequency. The peak at around 200°C is defined as depolarization temperature where the transition from ferroelectric to anti ferroelectric phase occurs due to absence of long range ferroelectric order [11] and the phase transition ferroelectric to paraelectric phase at 320 °C called as Curie temperature or phase transition temperature which involved the structural phase transition. The imaginary part ($\varepsilon^{//}$) i.e. dielectric loss is also follows the same behavior of ε_r. Baric *et al.* calculated the diffusivity value of phase transition by using modified Curie Weiss law

$$(1/\varepsilon - 1/\varepsilon_{m)} = (T - T_m)^{\gamma} / C ....(2.1)$$

and for NBT reported as $\gamma= 1.53$ for 10 kHz which proved that the phase transition is a diffused phase transition and this behavior is due to cation disorder at A-site [9].
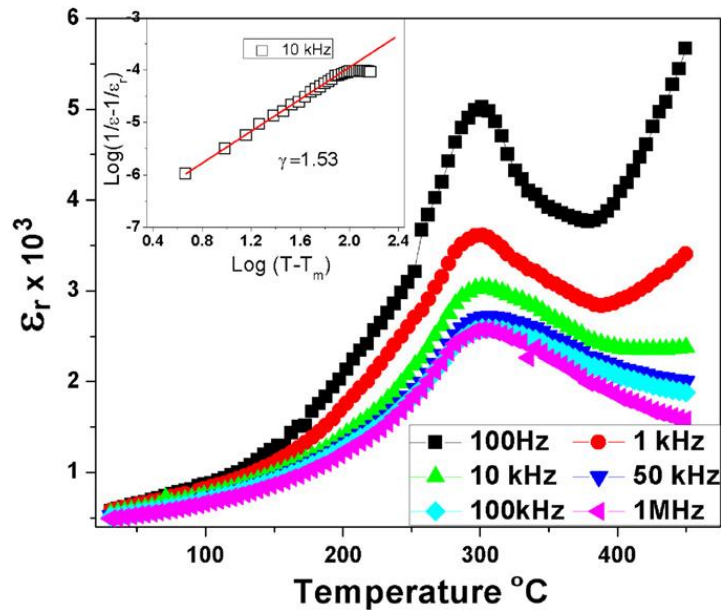
Fig 2.1: Dielectric constant studies of NBT from room temperature to 450°C at different frequencies (inset: modified Curie-Weiss plot of the same) [9]

These dielectric phase transitions are supported by temperature dependent Raman studies done by Viola *et al*. In this paper change in the dielectric constant was attributed to the change in the Raman mode intensities and splitting [11]. In this paper they reported the Raman modes at 270 cm^{-1}, 380 cm^{-1}, 520 cm^{-1} and 590 cm^{-1} in between 200 to 600 cm^{-1} range. Between room temperature to 125 °C, the mode at 270 cm^{-1} undergoes softening and intensity of this mode

decreases with increasing temperature and showing significant intensity after T_{max} suggesting the presence of polar nano regions, an in this region the ferroelectric phase is dominant. Above 125 °C this mode softening ceases suggests the increase in the spatial disorder, which leads to the shrinkage of polar clusters. The mode of 380 cm^{-1} show hardening with increasing temperature due to the change in the unit cell influences the octahedral framework, which leads to increased interaction between oxygen atoms [11].
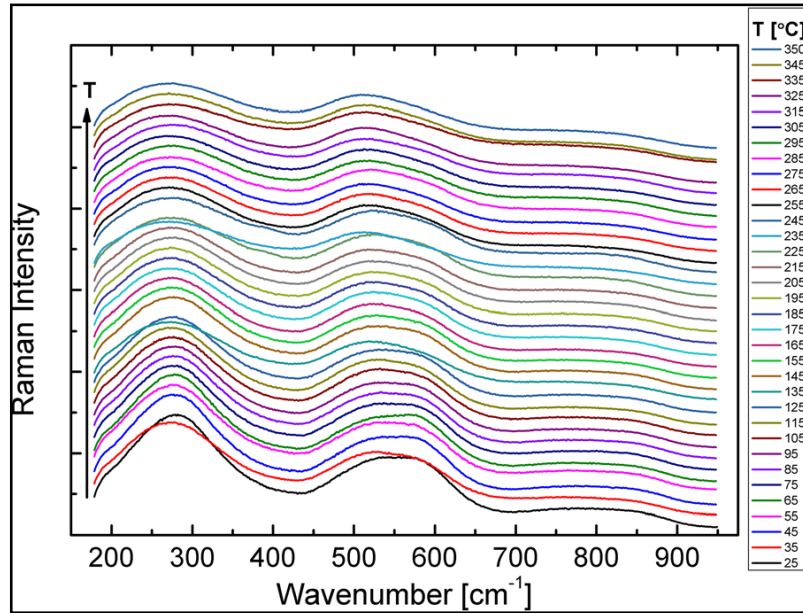
Fig2.2: Temperature dependent Raman spectrum of NBT [11]

Polarization vs. electric field (PE loop) characterization for NBT was done by Niranjan *et al.* in which they reported the coercive field E_c 65 kV/cm an remnant polarization as P_r = 38 $\mu C/cm^2$[12]. Due to this high coercive field these NBT ceramics are difficult to pole compared to other commercial piezo electric materials. To overcome this problem different dopants can be added to NBT and we can improve the piezoelectric properties (d_{33}). There are two types of dopants in NBT.

2.1.1 A site dopants:

La substituted NBT:

Aksel *et al.* substituted A-site by La^{3+} with 0.5, 1.0 and 1.5 at %. By this substitution the coercive field (E_c) decreased by 5 kV/mm and remnant polarization (P_r) increased by 5 $\mu C/cm^2$ and by 1.5 at% La substitution. The depolarization temperature (T_d) decreased

consistently as the La content increased, and 60 $^{\circ}$C decrease in T_d from unmodified to 1.5 at % La modified NBT .This feature is useful to the device application there is no change in the relaxor features of NBT by La substitution [13].
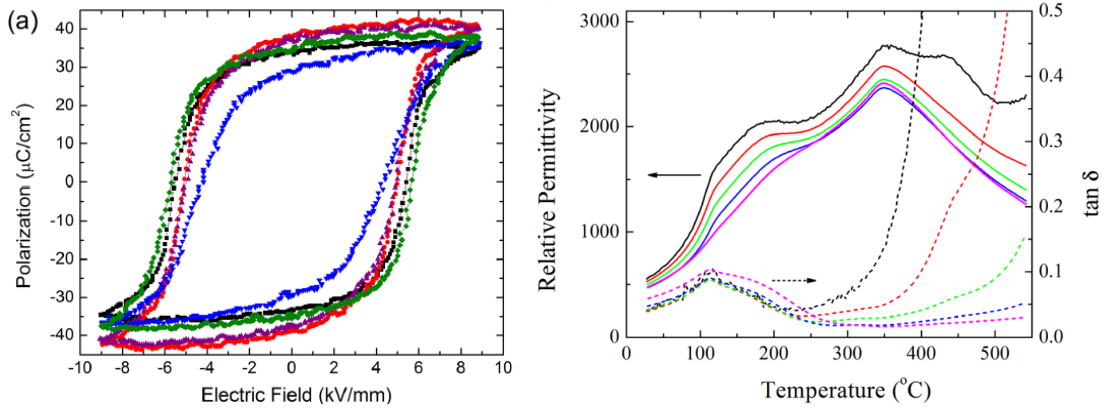
Fig 2.3 (a): PE loop of NBT and La substituted NBT [13], (b): Dielectric properties of NBT and La [13]

Fe substitution in NBT:

Elena Aksel *et al.* studied the effect of Fe^{3+} substitution in NBT. By substituting Fe local disorder decreases and the structure becomes closer to long range *Cc* structure. This can be correlated with the increased distortion of the unit cell leads to possible increase in octahedral tilting as observed in increasing lattice parameters. The addition of 0.5 and l at % Fe to NBT increases the depolarization temperature, and this is attributed to the defect dipoles that form with the addition of Fe to NBT which stabilize the ferroelectric order. Further Fe addition leads to a decrease in T_d, is due to limited poling owing to high conductivities of these samples [14].
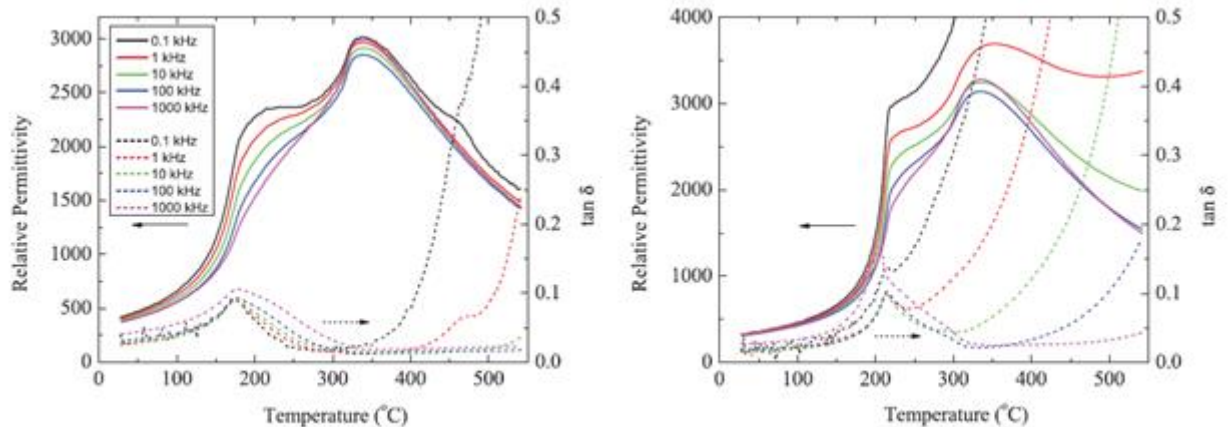
Fig 2.4: Phase transition plots of NBT and 0.5% Fe modified NBT [14]

2.1.2 B-site dopants:

In B site dopants are two types acceptor and donor dopants table shows the values of physical properties with different dopants. With the donor doping, E_c is decreased and P_r increased and with acceptor doping E_c is increased and P_r decreased [15].

Table2.1: Physical properties of NBT with different B-site substitutions [15]

Property	NBT	Donor		Acceptor		
	Ti^{4+}	Nb^{5+}	Ta^{5+}	W^{6+}	Mn^{3+}	Sc^{3+}
Ionic radius (Å)	0.605	0.64	0.64	0.64	0.64	0.64
d_{33}(pC/N)	74	87	84	84	66	77
k_p	0.17	0.17	--	0.16	0.13	0.16
Q_m	320	160	202	180	369	269
T_m (°C)	324	↑	-	↑	-	-
T_d (°C)	190	129	-	-	167	-
E_c @ 60Hz (k/cm)	~41	~24	~18	~20	-	-
P_r @ 60Hz (uC/cm^2)	~35	-	-	~40	-	-

Even though different substitutions were studied in NBT, there is no clear report on relaxor properties of NBT with Zr^{4+} substitution. Three people have reported about Zr substitution NBT, but they did not mentioned about the physical properties.

2.2 Literature review on NBT-BT solid solution:

The morphotropic phase boundary in NBT based solid solutions, attributed to the large piezoelectric properties. NBT-BT solid solution is one of the well-known materials with a morphotropic phase boundary (MPB) between rhombohedral phase of NBT and tetragonal phases of BT [16].
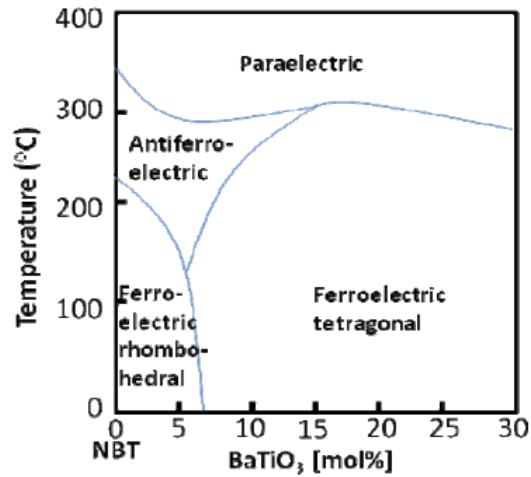
Fig 2.5: Phase diagram of NBT-BT [16]

Table 2.2: Piezoelectric properties of NBT-BT solid solution [17]

Compound	d_{33}(pC/N)	K_p	Tand (%)
NBT	64	302.6	1.752
(1-x) NBT-xBT, X=0.02	78	402	1.73
X=0.04	87	445	2.07
X=0.06	122	601	1.79
X=0.08	112	841	2.04
X=0.1	94	764	2.39

The below figure shows the phase diagram of NBT and BT. This MPB for NBT-BT is at 6-7 mol % of BT. In this region d_{33} values increase drastically compared to NBT (64 pC/N). The below table shows the increase in the piezoelectric properties with different compositions of NBT-BT solid solution [17].

Garg *et al.* discussed about the (1-x) NBT-xBT solid solution with different compositions by solid state sintering route. He reported the compositions of x= 0, 0.05, 0.065, 0.07 and 0.10. The below Fig. 2.6 shows the enlarged XRD patterns of (110), (111) and (200) reflections of (1-x) NBT-xBT. At x=0.05 composition, the XRD pattern is normal as NBT. From x=0.05 to 0.06 we can observe the changes in XRD patterns and all the peaks are singlet's at x=0.06. A sudden change in the XRD pattern occurs at x=0.07. The triplet nature of (110) and (200)

13

peaks can be explained as the coexistence of tetragonal and rhombohedral phases which is the feature of MPB system. The Fig. shows the piezoelectric coefficient (d_{33}) and maximum polarization (p_m) of NBT –BT ceramic. These properties shows a large values at x=0.06 - 0.07 region which are consistent with the above structural data from XRD [18].
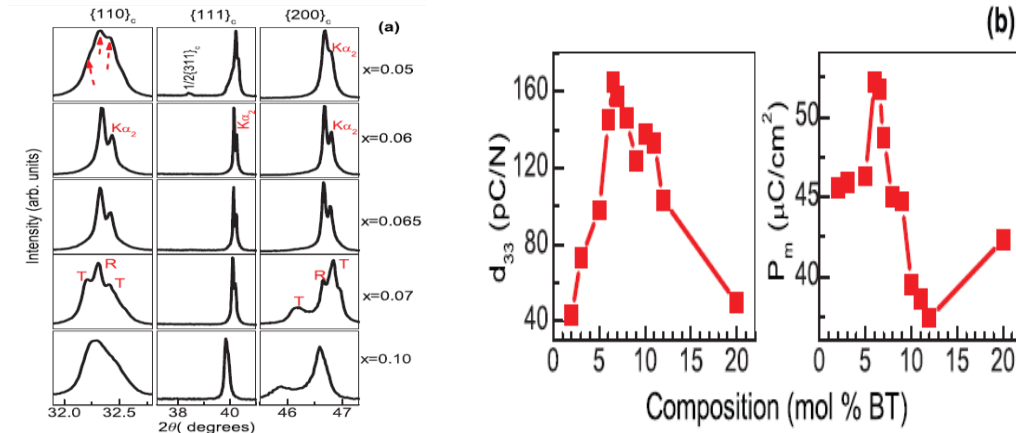
Fig2.6 (a): Enlarged profiles of (110), (111) and (200) peaks [18], (b) Composition dependence of Piezoelectric coefficient and maximum polarization of (1-x) NBT-xBT [18]

C. xu *et al.* studied the dielectric properties of the (1-x) NBT –xBT sold solution. The below Fig. 2.7 shows the dielectric constant vs. temperature plots for x=0.06 and x=0.12. This solid solution also exhibit two dielectric anomalies at 200 °C (Td) and 320 °C (T_m) like NBT. By adding BT to NBT T_d decreases and exhibit strong frequency dependence in x=0.06 which is reported as MPB. In x=0.12 composition this peak is very sharp which indicated the tetragonal side of MPB. T_m is also effected by Ba substitution as in x=0.06, the diffusivity of phase transition increased drastically to 2.02 compared to NBT as 1.55 and a slight decrement to 1.92 with further increase to x=0.12. This is concluded as 0.94 BNT – 0.06 BT ceramic i.e. at MPB has the maximum diffusivity value and this exhibits broad phase transition at around 320 °C because Na^+, Bi^{3+} and Ba^{2+} are randomly distributed in the 12 fold coordination sites so the observed diffuse phase transition at T_m is attributed to the disordering of A site cations [19].

The transition temperatures effected as T_d decreased by 168 °C to 105 °C at x=0.06 and increase to 194 °C with increasing x to 0.12. T_m is also decreased to 285 °C from 320 °C with x = 0.12 substitution. This decrease in T_d attributed as ceramics at MPB possess the lowest T_d, because of the oxygen octahedron tilting at this composition [19].

14
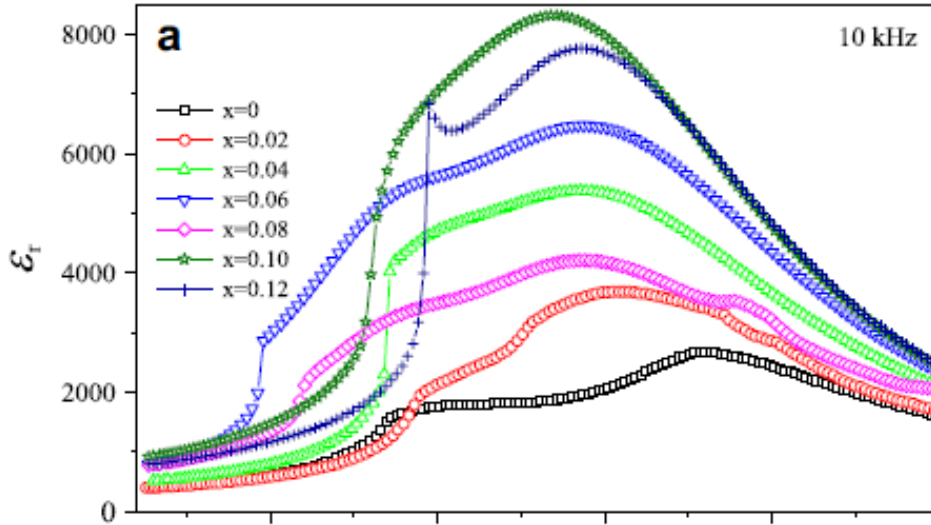
Fig 2.7: Dielectric phase transition plot of (1-x) NBT-xBT [19]

So this MPB of (1-x) NBT-xBT (x=0.06-0.07) is very useful for device applications due to high piezoelectric properties.

2.3 Objectives:

This work has been done with three major objectives.

1. To understand the relaxor feature of NBT by Zr – substitution. As NBT is showing diffused phase transition but absence of frequency dependence in T_{max} which is one of the relaxor feature. To improve this feature we substituted Zr^{4+} in NBT. The reason behind this explained below.

    Reason for Zr- Substitution:

    Zr^{4+} is isovalent with Ti^{4+} ions but heavier than Ti^{4+}. So oxygen hybridization will be high towards Zr because of its high atomic mass. So Zr-O bond is stronger than Ti-O and ZrO_6 octahedral distortion is less compared to TiO_6 octahedra. As a result the interaction between polar nano regions can be altered because of that relaxor feature can be improved.

15

2. For device application synthesis and characterization of NBT –BT solid solution for the enhancement of piezoelectric properties. As NBT – BT is well known material due to its high piezoelectric properties we tried to reproduce those results.

3. Testing of vibration sensor with the synthesized NBT for vibration sensing applications.

Chapter 3

Experimental Details

In this chapter the detailed synthesis procedure of sodium bismuth titanate [(Na$_{0.5}$Bi$_{0.5}$) TiO3) [NBT], Zirconium substituted NBT [Na$_{0.5}$Bi$_{0.5}$Ti$_{(1-x)}$ Zr$_x$O3, x = 0.05, 0.1], Barium titanate (BaTiO3) (BT), and NBT-BT solid solutions were clearly explained. Also basic working principles of structural, morphological and physical characterization techniques such as X-ray diffraction, Raman spectroscopy, scanning electron microscope, Piezo – d$_{33}$ meter and Impedance Analyzer were given briefly.

3.1 Synthesis

3.1.1 Synthesis of NBT and Zr substituted NBT through solid state reaction route:

Solid-state reaction route is most widely used method to synthesize polycrystalline ceramic compounds because in this route simple and cost effective. Oxides and carbonates are generally used as initial precursors. To synthesize compounds via solid state reaction route sufficiently high reaction (calcination) temperatures are required compare to wet chemical routes. This thermal energy will help to overcome the diffusion barrier and allows the ions to migrate through the rigid solid lattice. The reaction rate depends upon reaction atmosphere, structural aspects, surface area and reactivity of initial precursors [20]. In the present work to synthesize NBT and Zr substituted NBT the initial precursors such as Na$_2$CO$_3$, TiO$_2$, Bi$_2$O$_3$ and ZrO$_2$ with purity greater than 99.9% of SIGMA ALDRICH make were used. Initially all these precursors were weighed in stoichiometric proportion to obtain NBT and Zr substituted NBT. The stoichiometrically weighed powders were mixed and grounded in an agate mortar to obtain homogeneously mixed compounds. Homogeneously mixed powders were calcined at 800^{0}C for 4hrs to obtain single phase compounds. The phase purity of calcined compounds was confirmed through x-ray diffraction analysis. The phase pure calcined compounds were ball milled for 8hrs at 400 rpm using propanol as a medium to get the fine particles [Ball mill model: *FRITCH – PULVERISETTE 7 premium* Vials: Agate, Balls: Agate]. These fine

powders will enhance the sinterability of these compounds. After ball mill these fine powders were compacted in the form of cylindrical pellets using uniaxial hydraulic press. Prior to compaction Polyvinyl Alcohol (PVA) binder is added to these powders to enhance the formability. Then compacted pellets were sintered in a closed alumina crucible by covering the same composition powder over the pellets to reduce volatility of bismuth. Further the structural and phase purity of the sintered powders was confirmed through X-ray diffraction analysis. Morphology and vibration mode analysis of sintered samples were carried using Scanning Electron Microscope and Raman Spectrometer respectively. Dielectric measurements of sintered samples were carried out using Impedance Analyzer. Before taking dielectric measurements the samples were fine polished and electroded with silver paint for electrical contacts. Also the electroded pellets were poled under DC field to measure the piezoelectric properties of these ceramics. The figure 3.1 shows the flow chart of synthesis followed by characterization techniques.

This process involved several steps.

The flow chart of synthesis procedure is shown in Fig 3.1.
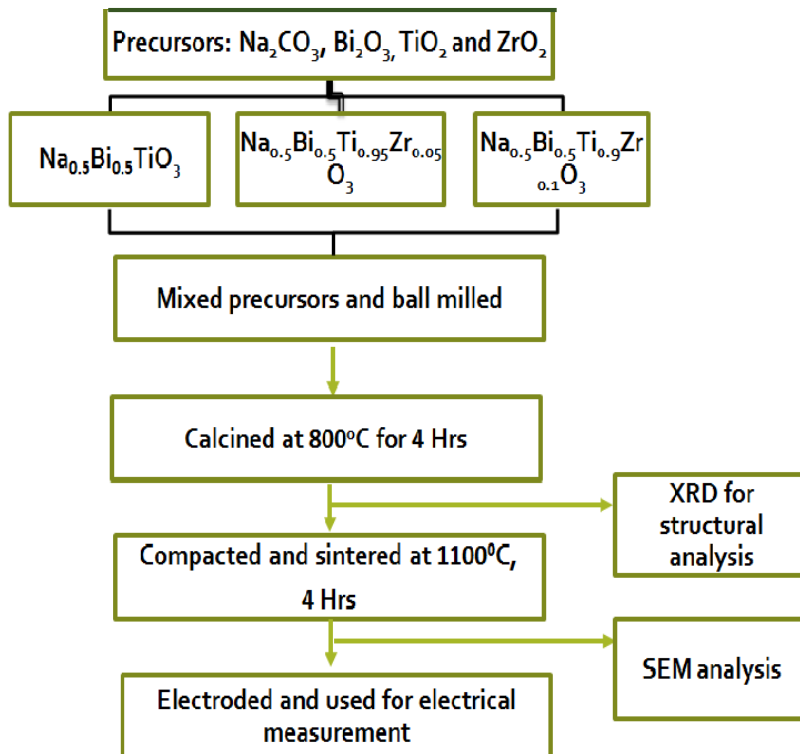
Fig 3.1: Flow chart of NBT and NBZT synthesis

Calcination:

Calcination is a thermal treatment process in solids in order to achieve thermal decomposition state for the required phase formation through interdiffusion between the precursors. The calcination temperature is usually below the lowest melting point among the precursors [20].

The manually mixed powders were calcined at 800 $^\circ$C in a closed alumina crucible. Calcination was done in muffle furnace with heating and cooling rate of 5 $^\circ$C / min and soaking time as 4 hr.
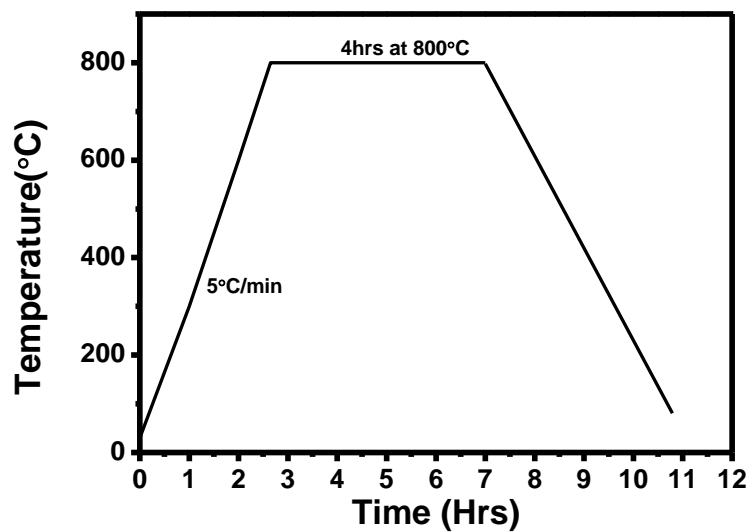
Fig 3.2: Calcination profile of the NBT precursors

Sintering:

Sintering is the densification process of a polycrystalline body with or without the presence of liquid phase to aid the transport of matter [22]. This transport of matter occurs by the diffusion of atoms, ions or molecules along surface, grains, grain boundaries and lattices. Initial bonding between the particles is the first step of sintering. Then neck growth followed by pore shrinkage and pore coarsening leads to densification. Sintering temperature, time and atmosphere can affect the microstructure i.e. particle size and shape of the product [6].

19
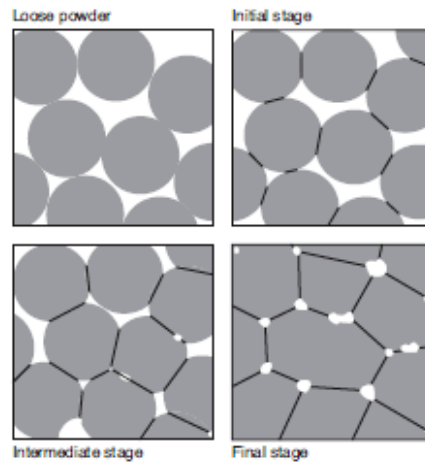
Fig 3.3: Schematic explain the stages involved in sintering mechanism [22]

Compacted pellets were covered with NBT powder to avoid bismuth volatility and sintered in a closed alumina crucible sealed with alumina paste to 1100 °C with heating and cooling rate as 5 °C/min in muffle furnace. At 300 °C soaked for 1hr for binder evaporation with heating rate of 3 °C/min.
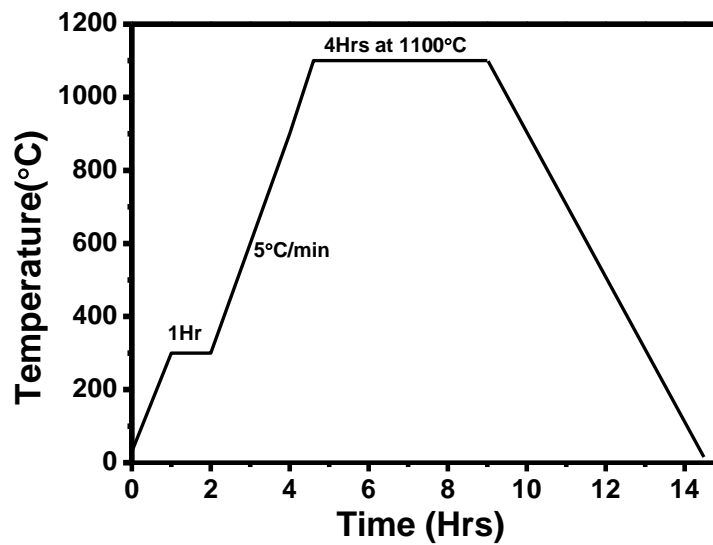
Fig 3.4: Sintering profile

Electric Poling:

Prior to any piezoelectric measurement, poling of the sample is needed. In all ferroelectric materials, dipoles are aligned in random directions. By applying electric field, which is equal or less than the coercive field (E_c), all the dipoles will try to align in the field direction. The

20

below figure explains about the alignment of dipoles by applying field. Generally poling procedure needs high temperature because by increasing temperature E_c of the material will decrease.
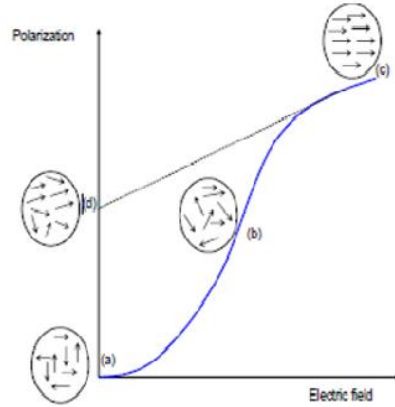
Fig 3.5: (a) Non polar state (b) Domains begin to align in field direction (c) Fully polarized state (d) By removing field i.e. at zero field remaining polarization (remnant polarization) [24]

3.1.2 Synthesis of Barium titanate:

Barium titanate was prepared by using Sol gel synthesis.

Sol gel method is a wet chemical synthesis technique for preparation of oxide gels ceramics at low temperatures. The sol gel process as the name implies, a transition from a liquid sol (colloidal solution) into a gel phase. This process involves hydrolysis and condensation of metal alkoxide followed by heat treatment at elevated temperature which induces polymerization producing a metal oxide network [25].

For the synthesis of $BaTiO_3$ through sol gel, barium carbonate ($BaCO_3$), titanium iso prop oxide (Ti (OCH $(CH3)_2)_4$), acetic acid (CH3COOH) and acetyl acetone ($C_5H_8O_2$) were used as precursors. The reason behind the selection of $BaCO_3$ is due to its high solubility compared to other materials. Barium carbonate is mixed with a 2 ml of acetic acid, stirred it for 30 - 40 minutes to prepare clear solution of Barium Acetate, then Titanium solution was prepared by mixing Titanium iso propoxide with acetyl acetone in 1:1 molar ratio. The reactions are shown below.

$BaCO_3 + 2CH_3COOH \longrightarrow Ba (CH_3COOH)_2 + CO_2 + H_2$ ………………… (3.1)

$Ti (OPr^i)_4 + C_5H_8O_2 (Acac) \longrightarrow Ti(OPri)_{4-x}(L)_x + x$ iPrOH…………………(3.2)

21

These prepared solutions mixed together and allowed for gelation at room temperature for 24 hour which allows desorption of solvent trapped in the polymeric network. Involving hydrolysis and condensation the BaTiO₃ gel was formed. This gel was calcined at 1000 °C for the phase formation and this phase purity was checked with XRD and used it for NBT-BT solid solution synthesis.

The below figure shows flow chart of Sol Gel synthesis for BT preparation.
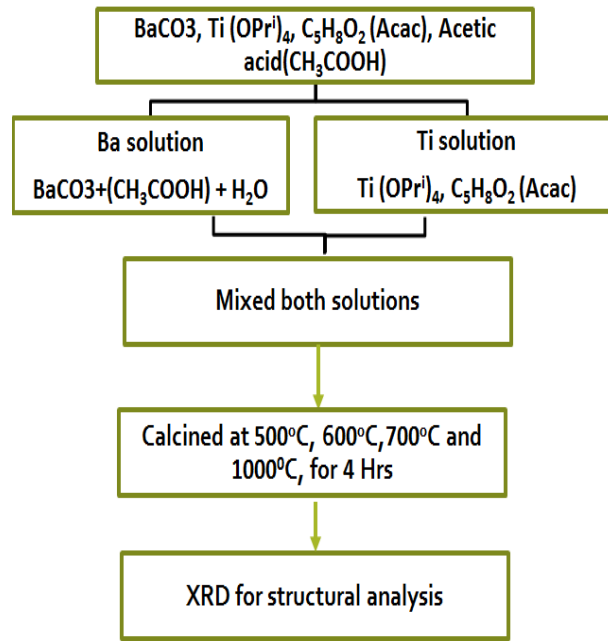
Fig 3.6: Flow chart of Barium titanate synthesis

Two major steps of sol gel synthesis are hydrolysis and condensation.

Hydrolysis:

The transition from sol to gel involves two steps. In hydrolysis process all the alkoxide groups are replaced by hydroxyl groups by the addition of water [25].

$$
\begin{array}{ccc}
\text{OR} & & \text{OR} \\
| & & | \\
\text{RO} - \text{M} - \text{OR} + \text{H}_2\text{O} \longrightarrow \text{RO} - \text{M} - \text{OH} + \text{R} - \text{OH} \\
| & & | \\
\text{OR} & & \text{OR}
\end{array}
$$
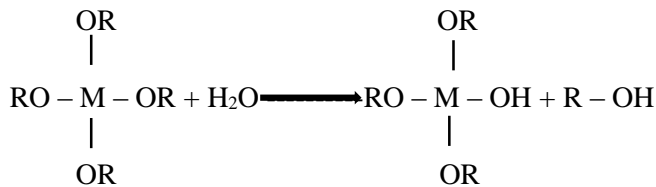
Ti iso propoxide is mixed with water, immediately Ti (OH) $_2$ will form. So to delay the hydrolysis process we used acetyl acetone as chelating agent.

Condensation:

Condensation reaction involves hydroxyl groups and result in M – O – M linkage which forms a 3D network by leaving water or alcohol as by product. From this reaction the viscosity of the sol becomes high through network formation and form gel.

$$
\begin{array}{ccc}
\text{OR} & \text{OR} & \text{OH} \quad \text{OH} \\
| & | & | \quad\quad | \\
\text{RO} - \text{M} - \text{OH} + \text{RO} - \text{M'} - \text{OH} \longrightarrow \text{HO} - \text{M} - \text{O} - \text{M'} - \text{OH} + \text{R} - \text{OH} \\
| & | & | \quad\quad | \\
\text{OR} & \text{OR} & \text{OH} \quad \text{OH}
\end{array}
$$
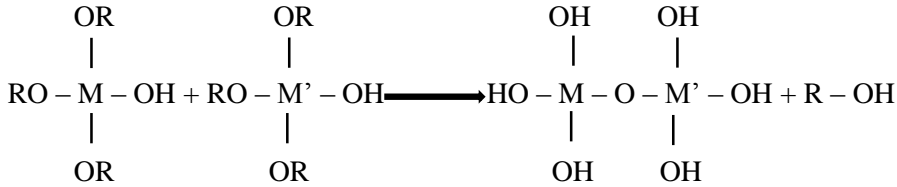
3.1.3 Synthesis of NBT-BT solid solution:

For NBT-BT solid solution preparation, NBT was prepared by SSR and BT was prepared by Sol gel route to improve the reactivity between the precursors.

The solid solution was prepared by using solid state route. Phase pure NBT and BT were weighed stoichiometrically and mixed together manually for 1 hour with acetone medium. Mixed powders were dried at room temperature and calcined at 800 °C. This powder was mixed with PVA binder, compacted by using hydraulic press with 2 tons load, and sintered at 1100 °C in a closed alumina crucible sealed with alumina paste in muffle furnace with heating rate of 2 °C/min up to 300°C and soaked for 1 hour at that temperature for binder evaporation and from 300 °C to 1100 °C heating rate as 5 °C/min. These sintered pellets were electroded and poled for electrical characterization.

3.2 Characterization techniques:

3.2.1 Density measurement:

Density measurements generally follow the Archimedes principle. According to this principle when a body immersed in a liquid loses weight by an amount equal to the weight of the liquid displaced.

$$
\text{Density of object} = \frac{Wa}{Wa - Ww} X\rho \quad \ldots\ldots\ldots\ldots\ldots\ldots\ldots\ldots\ldots\ldots\ldots\ldots\ldots\ldots\ldots\ldots(3.3)
$$

W_a= weight of object in air, W_w=weight water, ρ = density of water

3.2.2 X ray diffraction:

X ray diffraction is an eminent technique for structural characterization of crystalline materials. Each crystalline substance has its own XRD pattern which can be identified by using standard files (JCPDS). From this we can get the information of crystal structure, particles size, phase purity, and lattice parameters etc. The key principle of x ray diffraction is Bragg's Law.

This law is demonstrated by using two parallel planes in the crystal. The X rays incident on the set of parallel planes ABC and ABC' with an incident angle θ and scattered with same angle. If these scattered rays form two parallel planes are in phase, then they gives the peak with high intensities where as those reflected rays are out of phase will not give any intensities. The below figure shows the phenomenon of X ray diffraction [26].

$$n\lambda = 2d\sin\theta\ldots\ldots\ldots\ldots\ldots\ldots\ldots\ldots\ldots\ldots\ldots(3.4)$$

Here, λ = wavelength of the X ray, d = interplaner spacing, n= order of reflection and θ=angle of incidence.

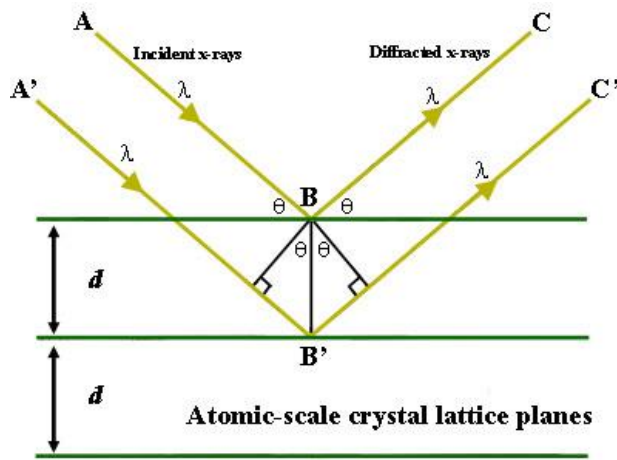**Fig 3.7: Schematic of Bragg's law**

PAN Alytical expert pro X ray diffractometer with copper Kα (λ=1.54 Å) radiation was used to investigate phase and crystal structure of the sintered ceramics.

24

3.2.3 Raman Spectroscopy:

Raman Spectroscopy is a vibrational spectroscopy which relies on inelastic scattering of light from the substance. When the light source interacts with a molecule, it polarizes the electron cloud. Then the molecule prompted to the virtual energy state where it has short life and comes back to higher or lower vibrational energy state by emitting phonons. In this process energy transfer can be done between photon and system. If the scattered photon has more energy than incident photon then it is called as Antistokes scattering. It has high energy and short wavelength. If the scattered photon has less energy than incident photon then it is called as stokes scattering. It has low energy and long wavelength [20]. The below figure explains the Raman scattering phenomena.
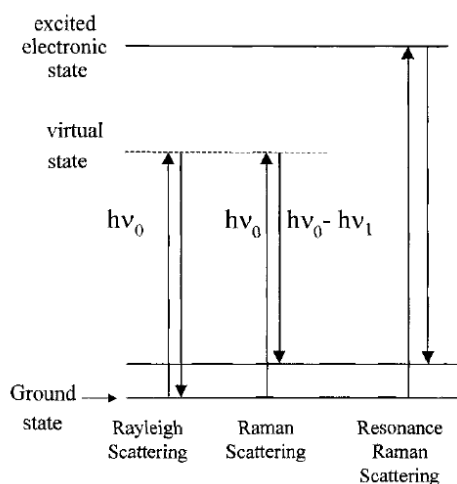

Fig 3.8: Raman scattering phenomenon [27]

Laser Micro Raman spectrometer (Bruker, Senterra) in a back–scattering geometry with an excitation source of 532 nm is used to obtain the Raman spectrum.

3.2.4 Scanning electron microscope:

Morphological studies were done by scanning electron microscope. It uses a focused high energy electron beam incidents on the specimen surface and generates a variety of signals because of electron-specimen interaction. Depending upon the required information these signals can be analyzed. Secondary electrons and back-scattered electrons are used for imaging and characteristic X-rays are used for elemental analysis [28].

All the samples were coated with gold by using sputter coater to make them conductive. Carl Zeiss Super 40 SEM was used for morphology and composition analysis studies.

Electrical measurements:

In this section phase transition studies, piezoelectric resonance, PE loop and piezoelectric coefficient characterizations were done.

3.2.5 Phase transition studies:

Every ferroelectric material will exhibits a phase transition from ferroelectric state to paraelectric state at certain temperature. Because of change in the dipolar displacement with temperature, so there will be change in the polarization and capacitance and related properties. This temperature where the material behaviour changes from ferroelectric to paraelectric state is called Curie temperature or phase transition temperature [6]. These studies were conducted by using precision impedance analyzer (Agilent 42941A). This system works based on the principle of Auto balancing bridge method which has frequency operational range of 40Hz to 110 MHz with high accuracy.

Electroded samples of NBT, NBZT5, NBZT10, NBT6BT and NBT8BT were used to measure the capacitance.

3.2.6 Piezoelectric resonance:

Every ferroelectric material is piezoelectric material. So they will exhibit piezoelectric resonance. When the applied frequency matches with the fluctuation frequencies of the ions, molecules, grains and grain boundaries in the material then they will vibrate with high amplitude [2].

These studies were done by using Precision impedance analyzer (Agilent 16034E).

3.2.7 Piezoelectric coefficient (d_{33}):

Piezoelectric coefficient was measured by using piezo test meter (PM 300). This instrument works based on the principle of piezoelectricity i.e. by applying mechanical stress to the system it'll generate electrical signals. In this system, mechanical stress is applied to the material by clamping it between the electrodes at required frequency. Then the material responds to the stress and generates electrical signals which will be compared with built in reference sample and directly displays the d_{33} value. Poled samples were used to measure the d_{33} value [9].

Chapter 4

Results and discussion of Zr substituted NBT

This chapter summarizes the results and discusses the outcome of NBT and NBZT ceramics with varying compositions.

4.1 XRD:

Fig. 4.1 shows the X-ray diffraction patterns of NBT, NBZT5 and NBZT10 ceramics prepared by solid state route sintered at 1100 $^\circ$C for 4 hours. These XRD patterns confirm the formation of perovskites with rhombohedral (R3c) crystal structure at room temperature [9]. NBT and NBZT5 compounds were formed as single phase and NBZT10 has a small amount of impurity. This impurity peak was attributed with the ZrO_2.

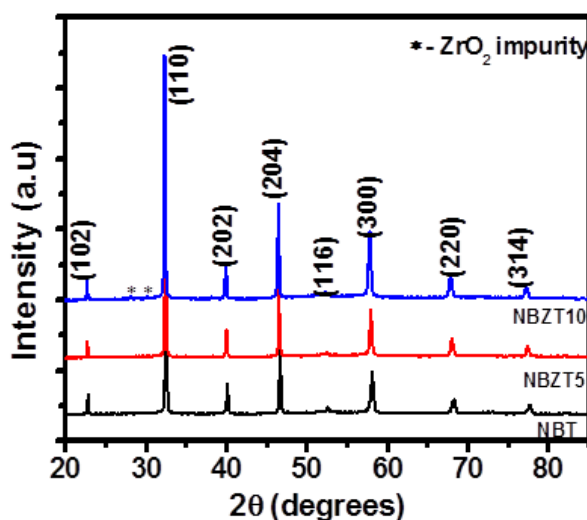**Fig 4.1 XRD pattern of sintered NBT, NBZT5 and NBZT10**

As the Zr content increases, the diffraction peaks were shifted towards lower Bragg angles which infer the expansion of unit cell. These changes are due to the substitution of higher ionic radii Zr^{4+} ion (0.72 Å) in Ti^{4+} site (0.605 Å) and confirm that Zr is substituted in Ti site. This shift in (1 1 0) peak is shown in Fig. 4.2.
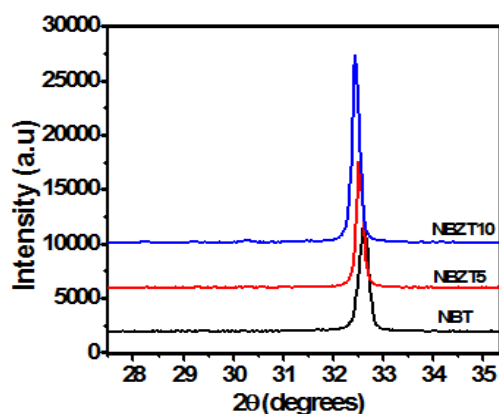
Fig 4.2: Magnified powder diffraction pattern indicating the shift in (1 1 0) peak

To extract the further structural information the diffraction peaks were analyzed by reitveld refinement method using Fullprof suite package. All room temperature data was modelled by using R3c space group. The χ^2 values show the goodness of fit and these refinement values are tabulated in table 4.1. NBZT 10 has impurity phase which corresponds to the decrease in the goodness of fit. The unit cell volume and lattice parameters are tabulated in Table 4.1, confirms the unit cell expansion and substitution of Zr^{4+} ion in Ti^{4+} lattice site.
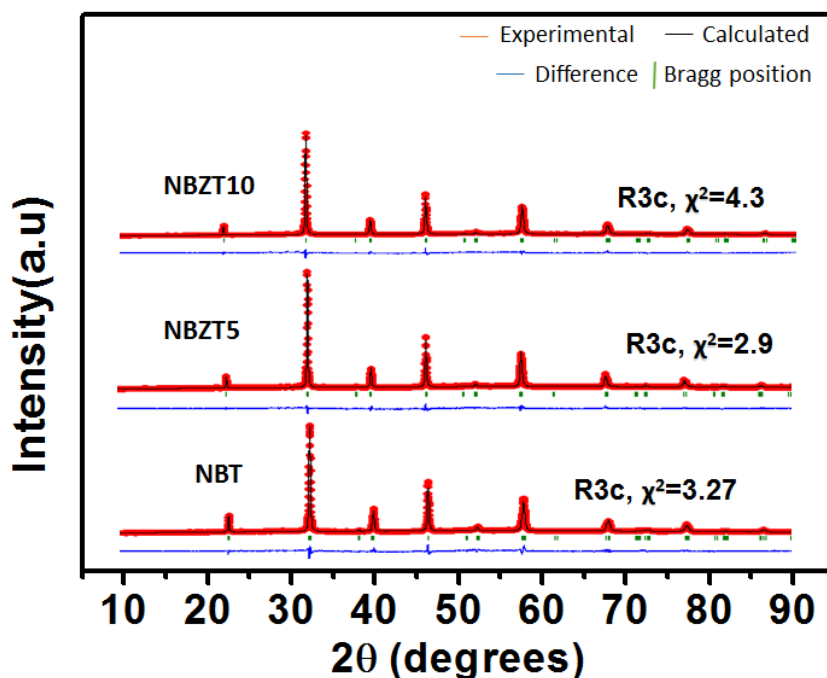

Fig 4.3: Rietveld refined XRD patterns

28

Table 4.1: Lattice parameters, unit cell volumes and fitting parameters from refinement

Material	a (Å)	c (Å)	Volume(Å)^3	χ^2
NBT	5.48544	13.49896	351.768	3.2
NBZT5	5.50346	13.50489	354.236	2.9
NBZT10	5.51337	13.53578	356.327	4.3

The peak around 38° corresponds to superlattice reflection of NBT compound which indicates the antiphase rotation a⁻a⁻a⁻ of the TiO_6 octahedra (characteristic tilting feature of R3c), confirms the space group as R3c rather than R3m. The weak intensity of this peak suggests the distortion from ideal cubic lattice is small and it decreases on increasing Zr content. The substitution of Zr does not introduce any additional structural phase transitions.

This data is further supported by Raman spectroscopy.

4.2 Raman spectroscopy:

To support the structural information from the XRD and to study the vibrational modes of the material, Raman spectroscopy was done to the pellets of pure NBT, NBZT5 and NBZT10. Fig 4.4 shows the Raman spectrum of NBT, NBZT5 and NBZT10 samples. The Raman spectrum of NBT is similar to the reported spectrum. There are 13 Raman active modes for Rhombohedral (R3c) phase and these modes were overlapped and appears as 6 Raman modes in the spectrum at 135 cm⁻¹, 276 cm⁻¹, 528 cm⁻¹, 580 cm⁻¹, 752 cm⁻¹ and 846 cm⁻¹ [11].

The mode at 135 cm⁻¹ is attributed to Na-O vibration. If we consider the mass of A-site ion in NBT, Bi is having higher mass than Na, so the mode corresponds to Bi-O vibration will be at lower frequencies and this can't be captured by the instrument. The mode at 276 cm⁻¹ corresponds to Ti-O vibration and it is sensitive to the local polar order, structural phase transitions [11]. Modes at 528 and 580 cm⁻¹ involves the polyhedral oxygen vibrations of TiO_6 octahedral stretching. This region is well known in perovskites oxides. Modes above 700 cm⁻¹ (752 cm⁻¹, 846 cm⁻¹) are related to the presence of oxygen vacancies while their intensity yields the vacancy concentration. This region is linked to the overlapping of A_1 (LO) and E (LO) [11].

We observed mainly two changes in the Zr substituted NBT from NBT.

1. Shift towards lower frequency by increasing Zr concentration, because of these higher ionic radii Zr^{4+} in Ti^{4+} site.

2. All the peaks were broadened and intensity decreased due to the substitution of Zr in Ti place leads to a local disorder without changing the symmetry. This was confirmed by XRD measurements that there is no change in the global symmetry but some local disorder is introduced by Zr substitution.
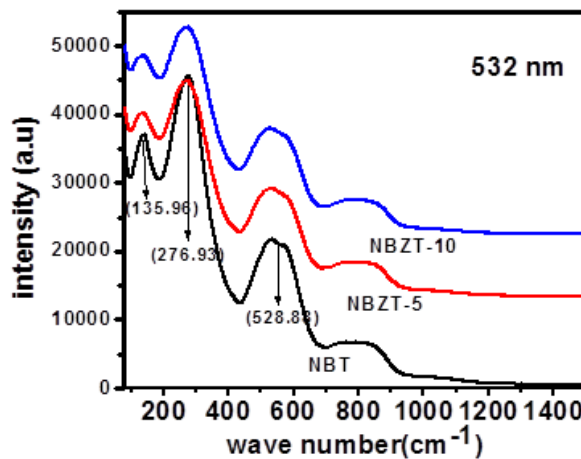

Fig 4.4: Raman spectrum of NBT and Zr substituted NBT

4.3 Scanning Electron microscope:

Fig. 4.5 shows the scanning electron microscope images of NBT, NBZT5 and NBZT10 sintered at 1100 °C for 4 hrs. These SEM micrographs shows the polycrystalline nature of the samples with a rectangular grains of different sizes randomly distributed on sample surface. Grains are well defined and sintering process (necking) is clearly visible. By Zr substitution the grains size significantly increases from 1 μm to 2 μm. The grain shape was also observed to change to rectangular shape by increasing Zr concentration. In NBZT5, NBZT10 micrograph, plate like structures was observed. The compositional analysis (EDX) revealed that those are Bismuth and sodium rich places. Fig 4.6 shows the EDX results of NBT, NBZT5 and NBZT10. In NBZT10 micrograph very small grains agglomerated with big grains were observed and those are explained as Zr rich regions .The contrast small dots on the grains of NBZT10 shows the presence of secondary phase. Over all sample morphology is densely packed and the relative density of the samples are around 90%. But few scattered pores are observed which indicates that there is certain degree if porosity in the samples.

In NBT, ring structures were observed which are evident to antiferroelectric phase transition. These structural domains are called as $180°$ domains. In NBZT5 and NBZT10 also we observed these structures which are confirming that there is no suppression in the antiferro electric phase transition at around 200 $°C$ by the substitution of Zirconium.
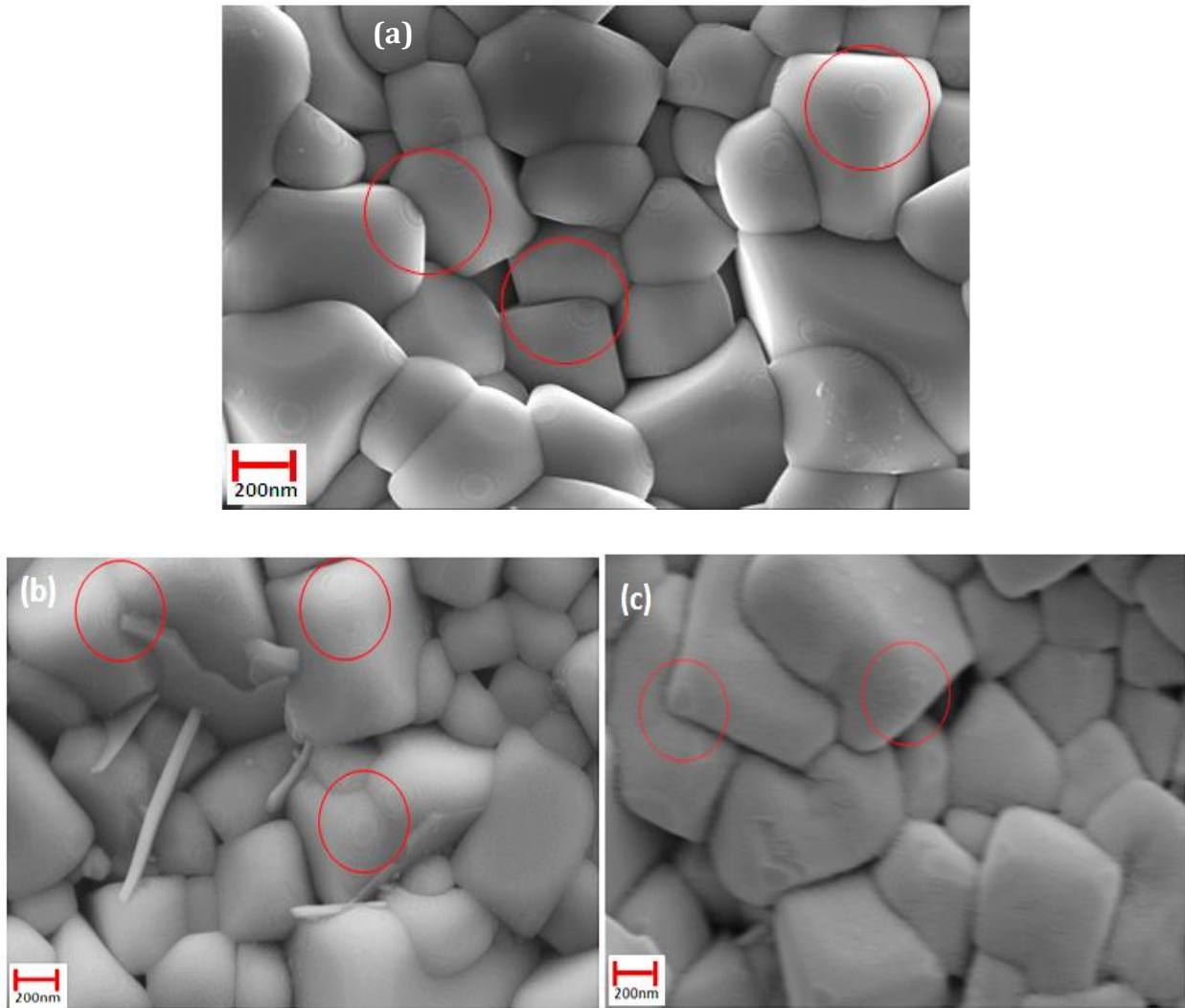

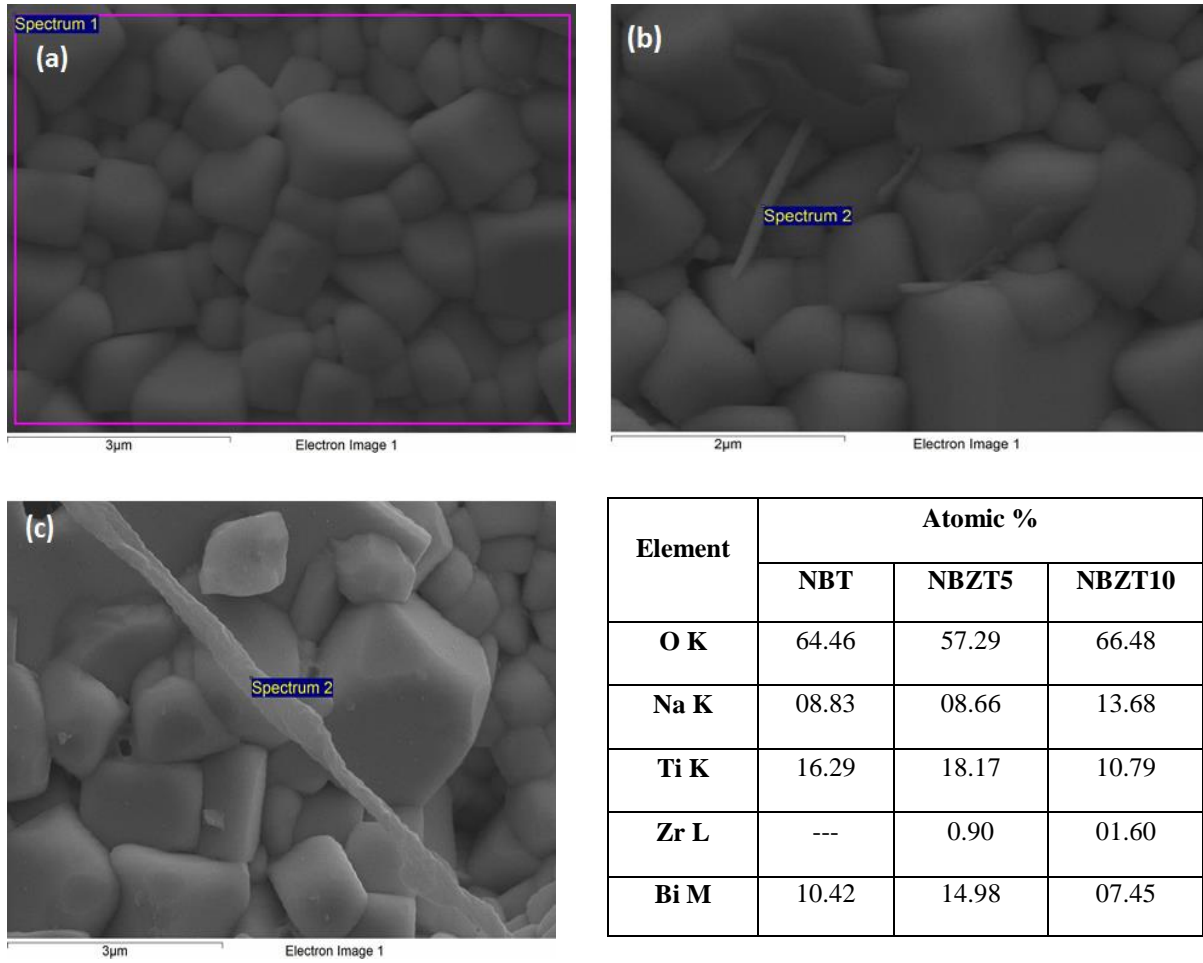**Fig 4.5: SEM micrographs of (a) NBT (b) NBZT5 (c) NBZT10**

Fig 4.6: EDX analysis of (a) NBT (b) NBZT5 (c) NBZT10

Element	Atomic %		
	NBT	**NBZT5**	**NBZT10**
O K	64.46	57.29	66.48
Na K	08.83	08.66	13.68
Ti K	16.29	18.17	10.79
Zr L	---	0.90	01.60
Bi M	10.42	14.98	07.45

4.4 Piezoelectric resonance and electromechanical coupling coefficient (k_p):

NBT, NBZT5 and NBZT10 materials were poled at 66 kV/cm field are measured the piezoelectric resonance frequency. Piezo electric resonance of NBT and Zr substituted NBT was measured by using Agilent probe (16304E) with frequency range of 40 Hz to 110 MHz. The below figure 4.7 shows the piezoelectric resonance curves of these materials. Pure NBT has 4 major modes at 570 kHz, 3.9 MHz, 12 MHz and 21 MHz. By Zr substitution the amplitude of the peaks decreased drastically. This might be because of the less distortion of ZrO_6 octahedra. These intensities were found to further decrease in NBZT 10.The modes at higher frequencies disappeared by Zr substitution.
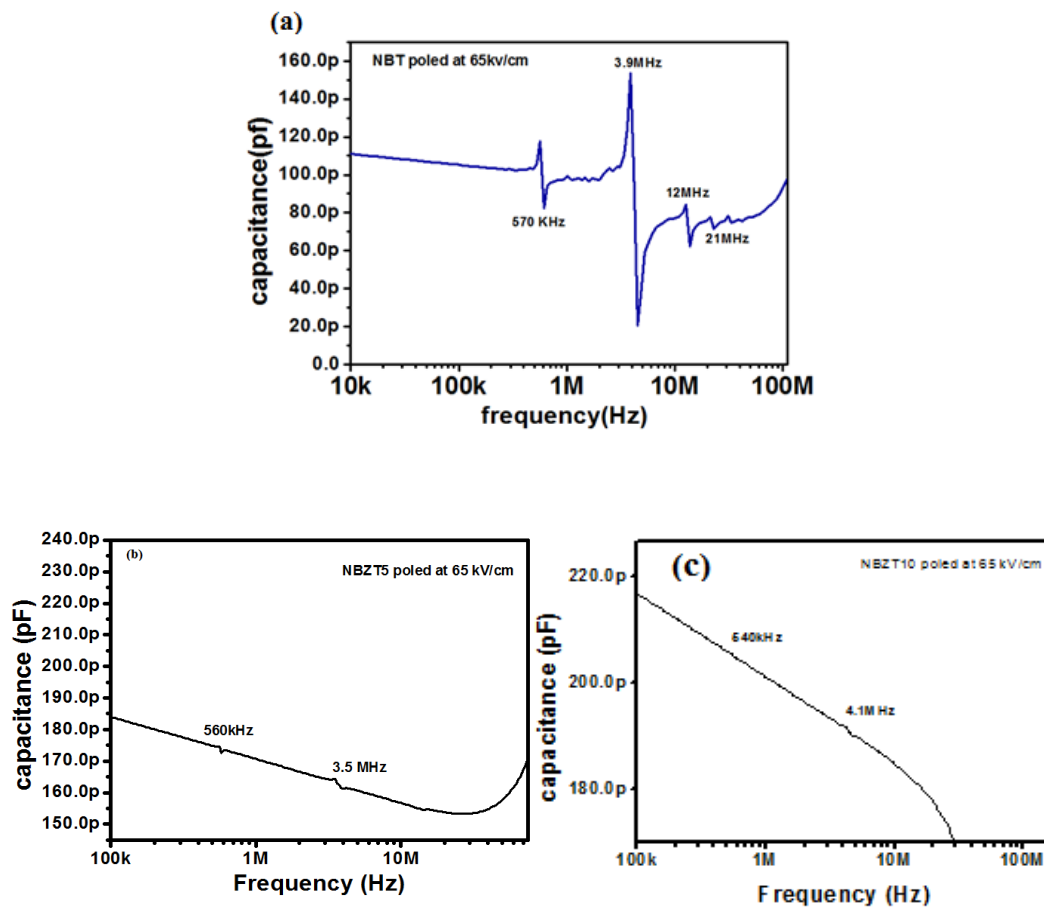
32

Fig 4.7: Piezoelectric resonance plots of (a) NBT (b) NBZT5 (c) NBZT10

Electromechanical coupling constant (k_p) is calculated by using resonance and anti – resonance method. These are calculated by using above piezo resonance graphs by using the formula.

$$k_p = \sqrt{\frac{2.51\,(f_a - f_r)}{f_a}}$$

……………………………………………..(4.1)

Here f_a = anti-resonance frequency, f_r = resonance frequency

The coupling coefficient decreased in NZBT5 compared to NBT as expected in piezo resonance measurement. But in NBZT10 K_p increased compared to NBZT5.

These values of coupling coefficient are tabulated in the below table:

Table 4.2: Calculated coupling coefficient (k_p) and d_{33} values

Material	k_p		d_{33} (pC/N)
	1St mode	2nd mode	
NBT	35.0	59.0	82.0
NBZT5	21.5	47.0	76.6
NBZT10	26	--	--

4.5 Piezoelectric charge coefficient (d_{33}):

Piezoelectric charge coefficient (d_{33}) was measured by using piezo test meter for the poled samples. . For NBT d_{33} value is 82 pc/N which is near to reported value. By Zr substitution this d_{33} value decreased because polarization is reduced which leads to the lower response less stress and low d_{33} value. These values are tabulated in Table 4.2.

4.6 Dielectric characterization:

NBT, NBZT5 and NBZT10 sintered and electrode pellets were used for dielectric constant measurements as a function of frequency and temperature. From these studies we can observe the phase transition and its nature, dielectric loss of the compounds.

For pure NBT we observed two phase transitions within the range of 50 °C – 400 °C at different frequencies. The dielectric anomaly at 200 °C represents the antiferroelectric to ferroelectric phase transition and this is called depolarization temperature (T_d). This transition attributed to the octahedral tilting present in the NBT system and loss of long range ferroelectricity. Other transition at around 310 °C involves antiferroelectric to ferroelastic phase transition with structural change from rhombohedral to tetragonal phase which is in agreement with literature. This is called as T_{max}, and at this T_{max} the dielectric constant is maximum and after that decreased which is the general property of the polar dielectric materials. This dielectric constant decreases with increasing frequency due to the dielectric relaxation. The nature of the phase transition is diffused, because of the distribution in size and strength of correlation between the polar nano clusters [11].
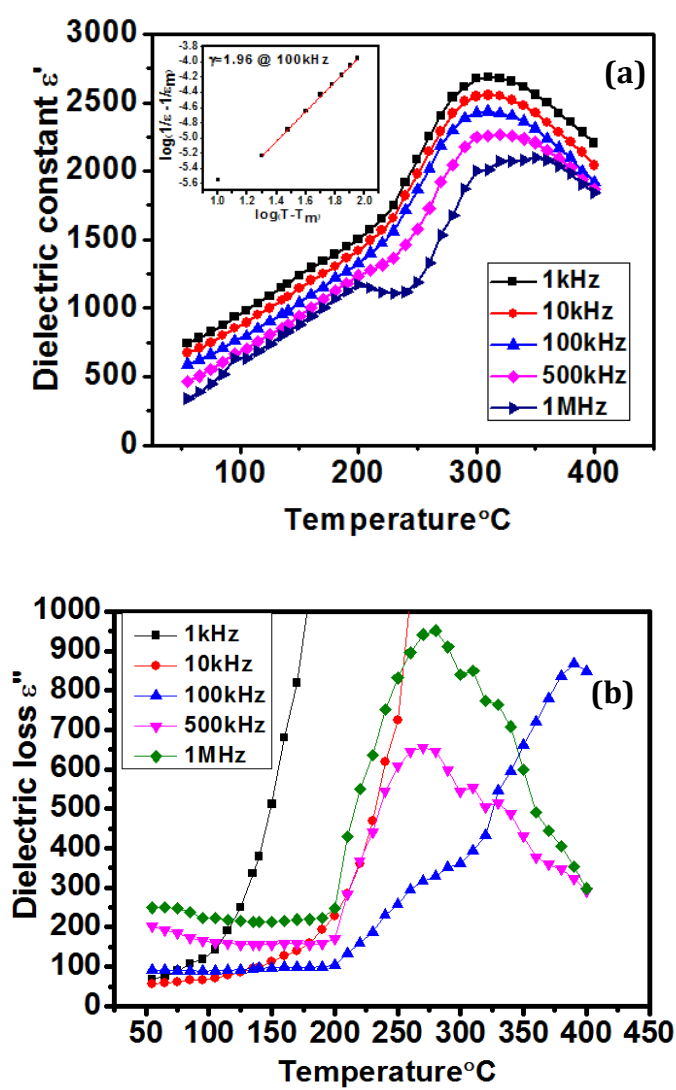
Fig 4.8: (a) Dielectric constant vs Temperature, Inset figure: Modified curie Weiss law plot
(b) Dielectric loss vs Temperature at frequencies

This diffusivity of phase transition can be calculated by using modified Currie Weiss law. For NBT this diffusivity $\gamma=1.92$ at 100 kHz. The dielectric constant of NBT at 100 kHz is 2437. This graph is shown in inset of Fig 4.8 (a).

The dielectric loss will also follows the same nature of dielectric constant, shown in fig 4.8(b) the loss is very high at low frequencies and after that it followed the property like with increasing frequency loss is increasing because of the insufficient relaxation time of the dipoles.

NBT with Zirconium Substitution:

By substituting with Zr the dielectric constant decreased drastically to 1818 (at 100 kHz) due to the decrease in the polarization with Zr substitution. The T_{max} is increased slightly to 325 °C. Initially we observed the frequency dispersion in T_{max} due to the change in the strength of interaction between polar nano regions. Because by Zr^{4+} substitution, ZrO_6 octahedral distortion is less compared to TiO_6 octahedral. So there are the regions with different strength of polarization apart from the regions of A - site cationic disorder. This effect is resulted as frequency dispersion in T_{max} and this can be proved by using Vogel fulchur law which is shown in Fig 4.9. The below figure shows the dielectric constant vs temperature plots of NBZT5 and NBZT10.
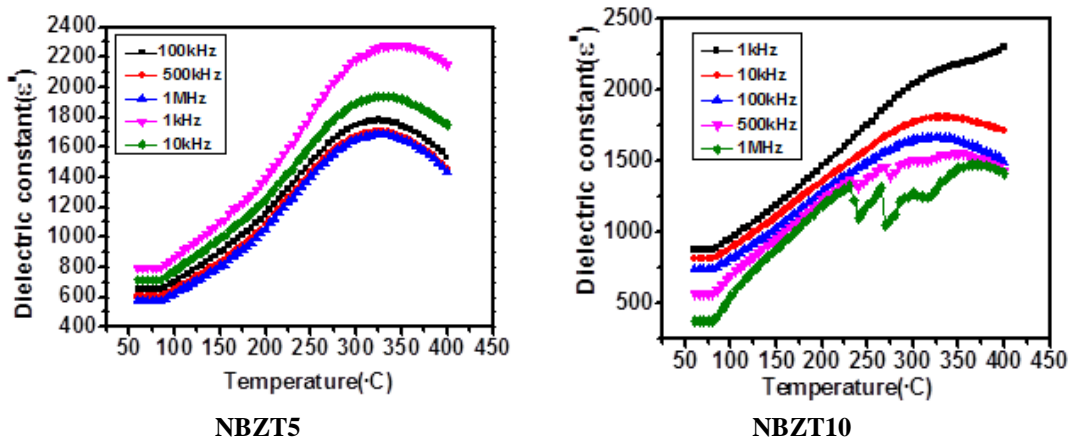

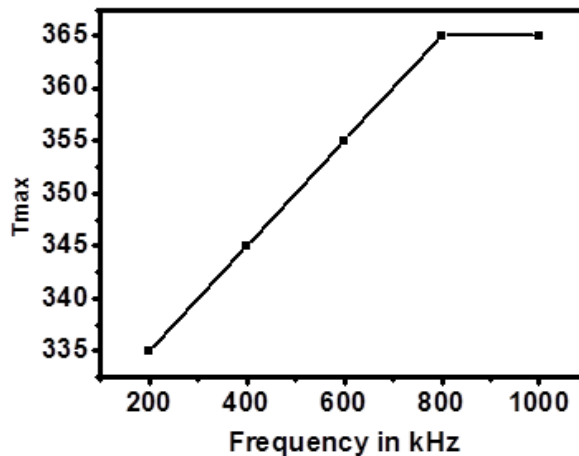| NBZT5 | NBZT10 |

Fig 4.9: Dielectric constant Vs temperature

Fig 4.10: Vogel fulchur law for NBZT10

We repeated the same measurement by changing the electrode to study the external effects. The below figure 4.11 and figure 4.12 shows the repeated data of dielectric in which this frequency dispersion disappeared in both the compositions (NBZT5, NBZT10). This might be due to the change in the interface between sample and the electrode, which could affect the measurements due to interface. This change can be observed in the plots below. Inset figures in dielectric constant graphs are diffusivity plots of NBZT5 and NBZT10.
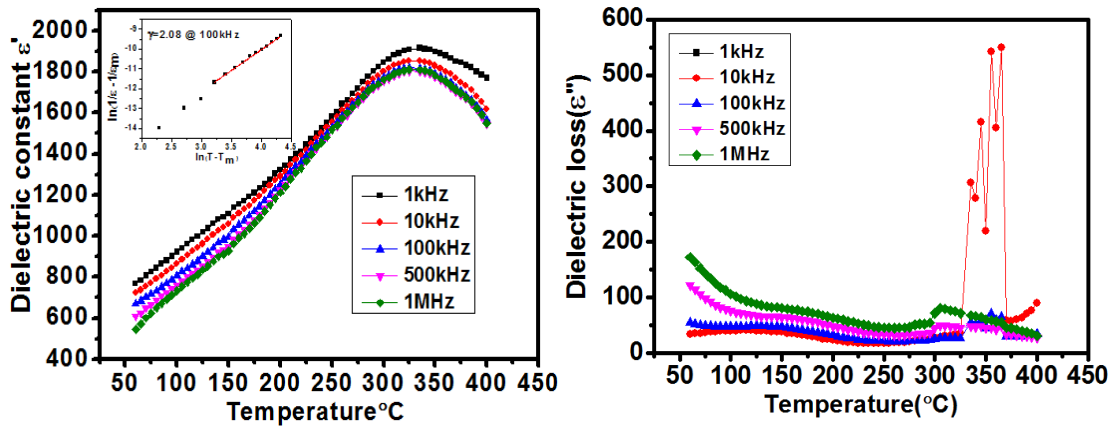

Fig 4.11: Dielectric constant and Dielectric loss Vs temperature plot of NBZT5, Inset figure: Modified curie Weiss law plot
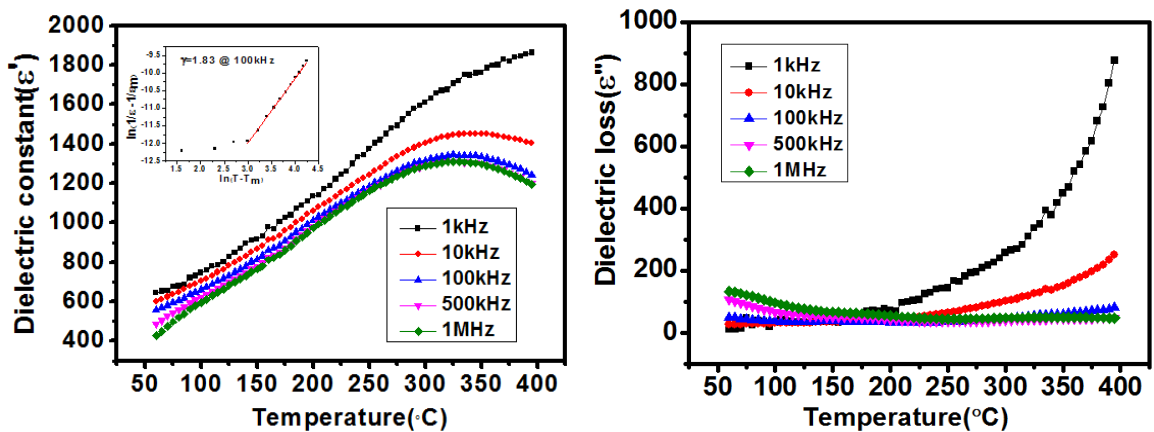

Fig 4.12: Dielectric constant and Dielectric loss Vs temperature plot of NBZT10, Inset figure: Modified curie Weiss law plot

So there is a frequency dispersion introduced by Zr substitution in NBT in the first measurement and it was not repeated in other measurements. Dielectric constant is decreased with increasing Zr concentration. The depolarization peak at $200\,^0C$ temperature was observed as decreasing with Zr substitution which is the evidence of presence of AFE transition and this is supported by SEM results with the $180^°$ domains presented in the NBZT5 and NBZT10.

The dielectric loss also followed the same nature of dielectric constant except at low frequency (1 kHz) and this loss increased by increasing frequency, compared to NBT loss is decreased in the Zr substituted NBT. The behaviour of phase transition is broad in all compositions and there is no considerable change in the diffusivity, these values are for NBZT5 $\gamma = 2.02$ at 100 kHz and for NBZT10 $\gamma = 1.83$ at 100 kHz.

Chapter 5

Results and discussion of NBT-BT solid solution

5.1 XRD:

In this solid solution NBT was prepared by solid state route and BT was prepared by sol gel synthesis. Both phase pure compounds are used for the preparation of NBT – BT solid solution. The below Fig 5.1 shows the XRD patterns of NBT and BT which are the starting materials.
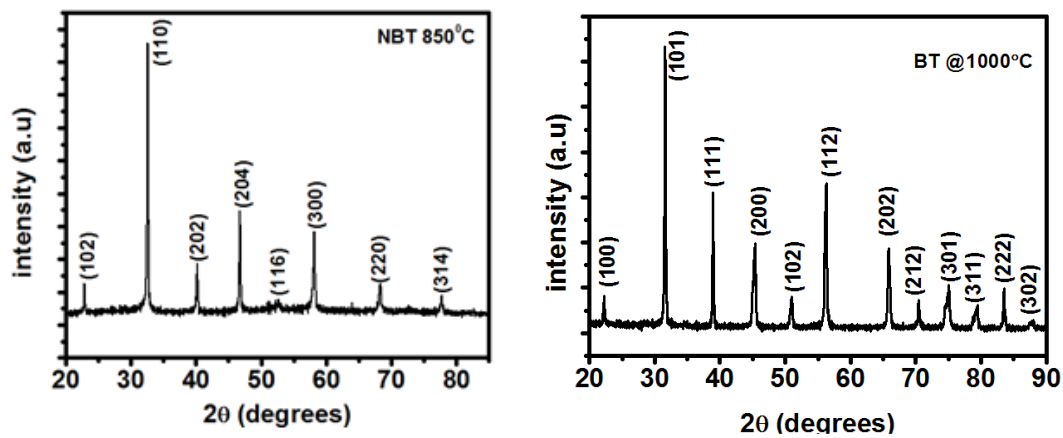

Fig 5.1: XRD patterns of NBT and BT

From the above XRD patterns we can observe the phase purity of NBT and BT and NBT with Rhombohedral (R3c) crystal structure and BT with Tetragonal (p4bm) structure.

Fig 5.2 shows the XRD patterns of (1-x) NBT –x BT (x=0.06, 0.08) prepared by conventional solid state route which are sintered 1100 °C for 4 hrs. These XRD patterns confirm the formation of single phase perovskite with room temperature crystal structure as rhombohedral

(R3C). The narrow and symmetric XRD patterns of NBT-BT compounds indicated the homogeneity and good crystallization.
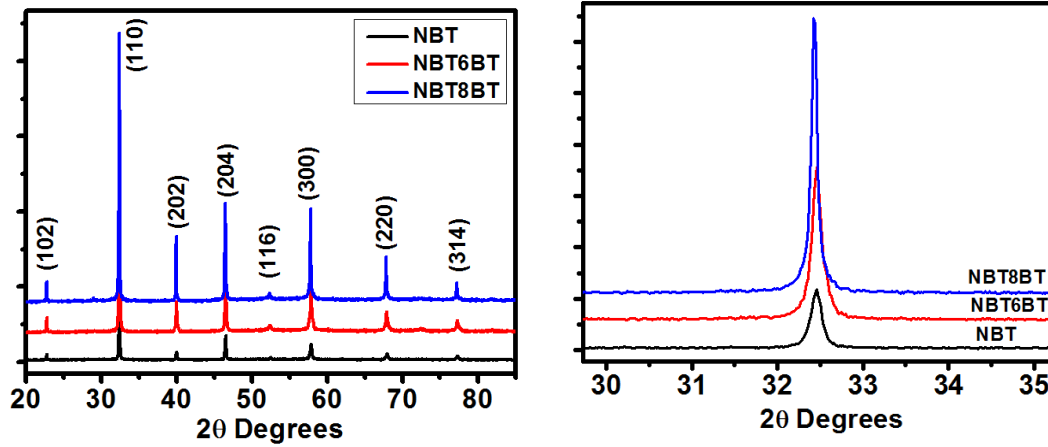

Fig 5.2: XRD patterns of NBT-BT solid solution and Shift in (110) peak

With increasing x value (Ba concentration) peaks shift slightly towards lower Bragg angles which means that lattice parameters and unit cell volume also increases. This is attributed that Ba^{2+} is diffused into the NBT lattice sites. This is because of the substitution of higher ionic radii Ba^{2+} (1.36 Å) in the lower ionic radii Na^{+1} (1.02 Å) or Bi^{3+} (1.03 Å), due to this inter planner spacing will increase as a result peaks shifts towards lower angles. The peak intensities increased with Ba^{2+} substitution [19].

The characteristic feature of NBT i.e. super lattice peak became invisible with Ba^{2+} substitution. These super lattice peaks are due to the octahedral tilting with respect to adjacent octahedrons (oxygen). Due to the lower scattering power of X rays and the magnitude of the tilt is small, sometimes it is difficult to observe these peaks. According to literature there is a MPB between Rhombohedral (NBT) and Tetragonal (BT) at BT concentration as (x=0.06 – 0.07). These structural changes can be observed by the splitting in the characteristic peaks. But in our data we did not observed any structural changes in both the compositions (0.94NBT-0.06 BT) and (0.94NBT-0.08 BT) [19].

5.2 Scanning Electron Microscope:

The SEM micrographs indicate the polycrystalline nature of the compounds with distorted rectangular shapes. The overall microstructure is looking dense and the density of these samples is at around 96 %. The sintering mechanism i.e. necking can be observed with well-

defined grain boundaries. The below Fig. 5.3 shows the scanning electron microscope images of NBT6BT and NBT8BT.
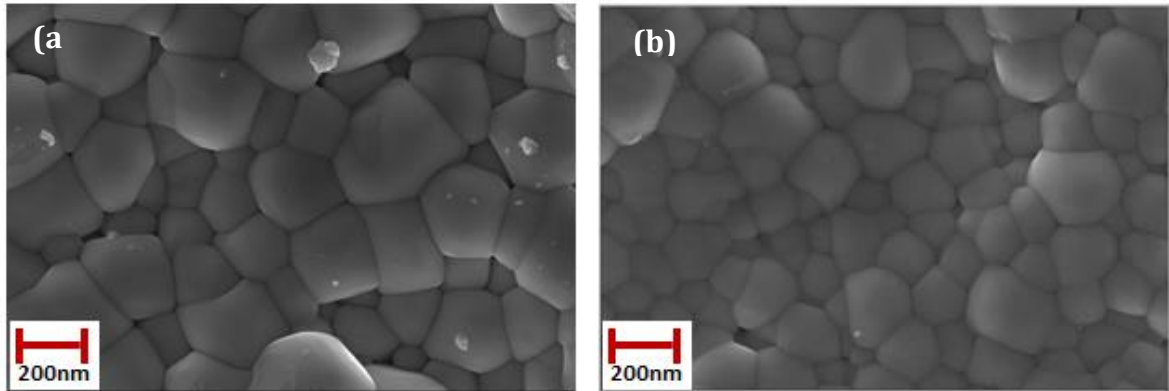

Fig 5.3: SEM micrographs of (a) NBT6BT (b) NBT8BT

The grain size varied from 100 nm to 1μm because the starting materials NBT was synthesized by solid state route which gives the grain size as in μm range and BT was synthesized by sol gel with nm grains, because of this there is a huge change in the grain sizes. The compositional analysis was done at different places in 0.94 NBT-0.06BT and 0.94 NBT-0.06BT showed the elements are in the normal expected range.

5.3 Resonance – antiresonance studies and electromechanical coupling coefficient (k$_p$):

These materials are poled at 60 kV/cm field and used for piezoelectric resonance measurements. These measurements were done by using Agilent probe (16304E) with frequency range of 40 Hz to 110 MHz. The below Fig.5.4 shows the piezoelectric resonance frequencies NBT6BT and NBT8BT. In NBT6BT has four major modes at 540 kHz, 1.4MHz,2.2 MHz and 3.4 MHz and in NBT8BT total five modes were observed at 80 kHz , 470 kHz , 750 kHz , 1 MHz and 2,1 MHz which is attributed to the near to MPB region.
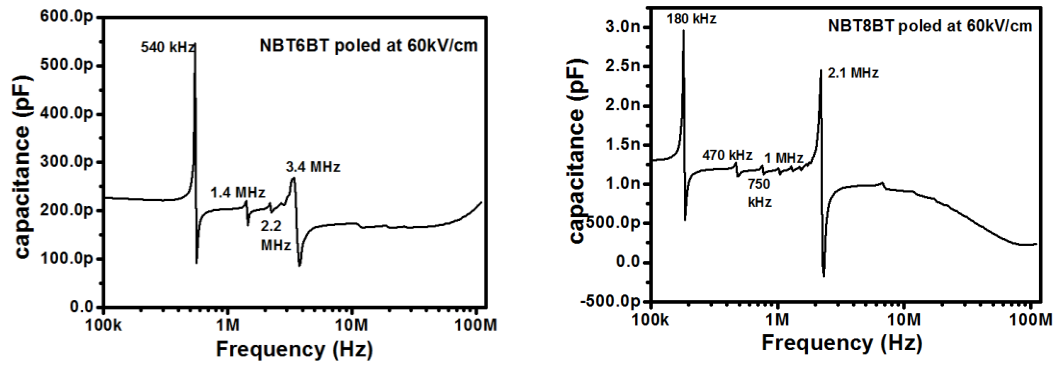
Fig 5.4: Piezoelectric resonance frequency plots of NBT6BT and NBT8BT

Electro mechanical coupling coefficient was calculated by using resonant and antiresonant method. These values are tabulated in table 5.1. The coupling coefficient is of NBT8BT is high compared to NBT6BT which is again indicating that NBT8BT is near to MPB regions compared to NBT6BT.

Table 5.1: Piezoelectric resonance frequency and k_p values

Mode	NBT6BT		NBT8BT	
	f_r	k_p	f_r	k_p
1st	540.0 kHz	26.0	180.0 kHz	22.2
2nd	1.4 MHz	22.2	470.0 kHz	35.7
3rd	2.2 MHz	31.3	750.0 kHz	30.0
4th	3.4 MHz	50.0	1.0 MHz	34.0
5th	--	--	2.1 MHz	35.7

5.4 Dielectric Studies:

The below figure shows the variation of dielectric constant and loss with temperature at different frequencies. The dielectric response of NBT6BT and NBT8BT exhibits the diffuse phase transition like NBT, and here also we observed to anomalies as T_d and T_m, where T_d corresponds to the transition from ferroelectric to antiferroelectric state.
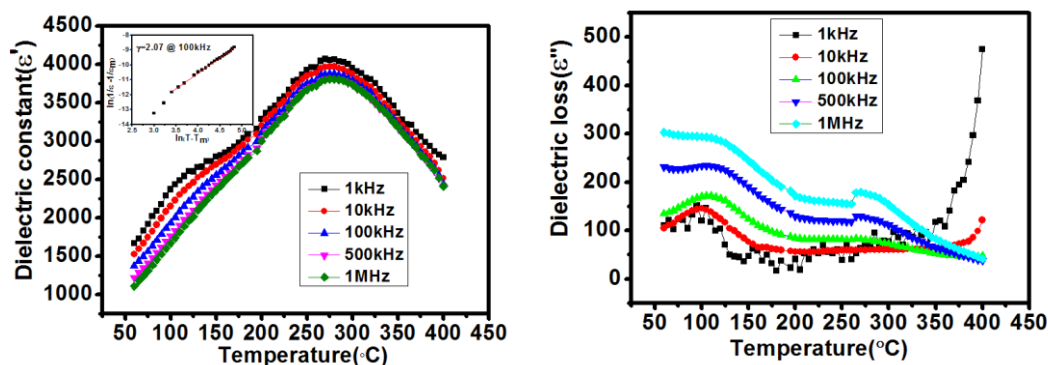
Fig 5.5 (a): Dielectric constant plot of NBT6BT, (b): Dielectric loss plot of NBT6BT
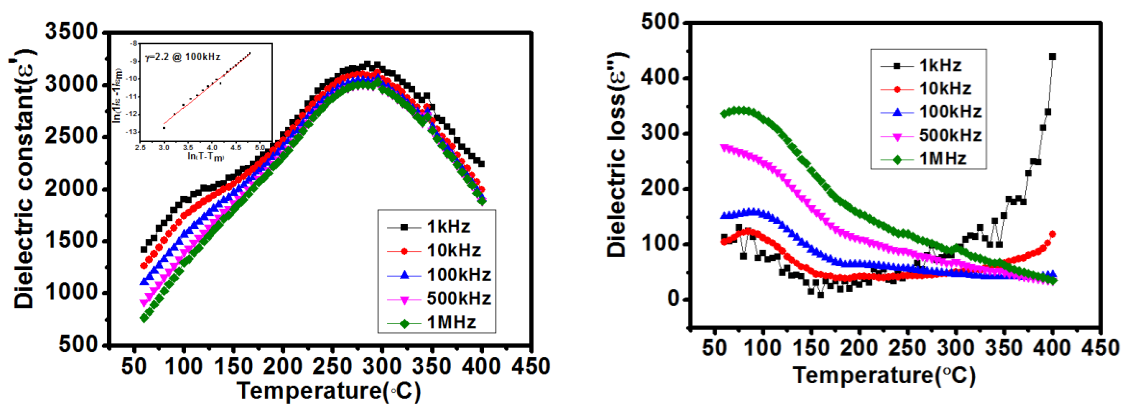

Fig 5.6: Dielectric property of NBT8BT

Fig 5.6 (b): Dielectric loss plot of NBT8BT

At T_m there is a structural phase transition along with ferroelectric transition which is broad. In NBT-BT the values of T_d and T_m are low compared to NBT. The improvement of piezoelectric properties depends upon the sufficient reorientation of 90° domains. Lower T_d means lower stabilities, which favors the easy reorientation of 90° domains and results high piezoelectric properties. So in NBT-BT because of the decrease in T_d from 200 °C to 120 °C in NBT8BT provide the better piezoelectric properties than NBT6BT. The diffusiveness of this relaxer ferroelectrics are calculated by modified Curie –Weiss law where there is a slight increase in the diffusivities. These values are tabulated in table 5.2. The inset figures in dielectric constant vs. temp plots show the modified Curie Weiss law plots.

The dielectric constants values are also increased drastically. These values are tabulated in below table.

Table 5.2: Transition temperatures, dielectric loss and diffusivity values

Material	T_d (°C)	T_m	Dielectric constant at 100 kHz	γ	Loss at 10 kHz
NBT	200	310	2437	1.90	800
NBT6BT	120	275	3881	2.07	120
NBT8BT	100	280	3044	2.20	150

The decrease in T_d and T_m, dielectric loss and increase in the dielectric constant are attributed that NBT-BT solid solution is better for device applications compared to NBT.

Chapter 6

Testing of NBT as a vibration sensor

6.1 Introduction:

Vibration sensor comes under accelerometer. Accelerometers are the most common dynamics sensors capable of a vast range of sensing. These are used to measure the mechanical variables i.e. acceleration, vibration and mechanical shock. There are several types of accelerometer based on the working principle i.e. piezoelectric, piezoresistive and piezocapacitive accelerometers [29]. In these piezoelectric accelerometer is the most common. It works based on piezoelectric effect. In this accelerometer a mass is attached to a piezoelectric which is mounted on base materials. The stress is generated on the crystal as result of the mass imposing a force on the crystal [32]. Due to this charge is accumulated on the crystal (piezo electric effect). Electrodes will collect this charge and transmit it to a signal conditioner; there it will be amplified into either voltage or current. This piezo electric accelerometer obeys Newton's second low (F=ma) as charge generated is proportional to the applied force. The below figure shows the one variety of configuration [31].
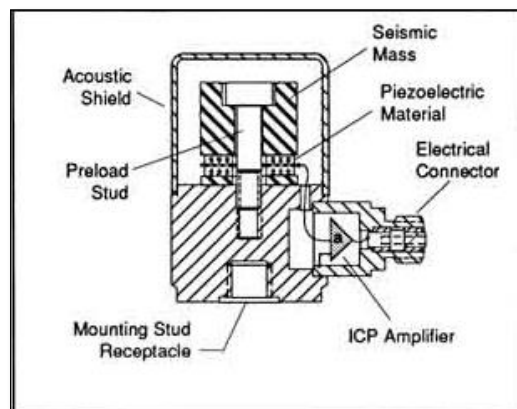

Fig 6.1: Compression model of piezoelectric accelerometer [31]

This performance of piezoelectric accelerometers is affected by resonance frequency, mass interface and other external factors. For sensor applications resonance frequency of a

piezoelectric material is an important factor, because the maximum usage limit of the sensor will be decided by this factor [5]. Below or above the resonance frequency we can use the sensor and at resonance frequency loss will be very high so we can't use the sensor at that frequency [29].

6.2 Testing the vibration sensor:

The NBT pellet which was synthesized by solid state route is used for this sensor preparation. This pellet was poled at 45 kV/cm. After mounting the sample on a base material, checked the resonance frequency by using 50 g and 100 g masses. There is no change in resonance frequency by increasing weight. The below figure shows the Piezoelectric resonance plots of NBT.
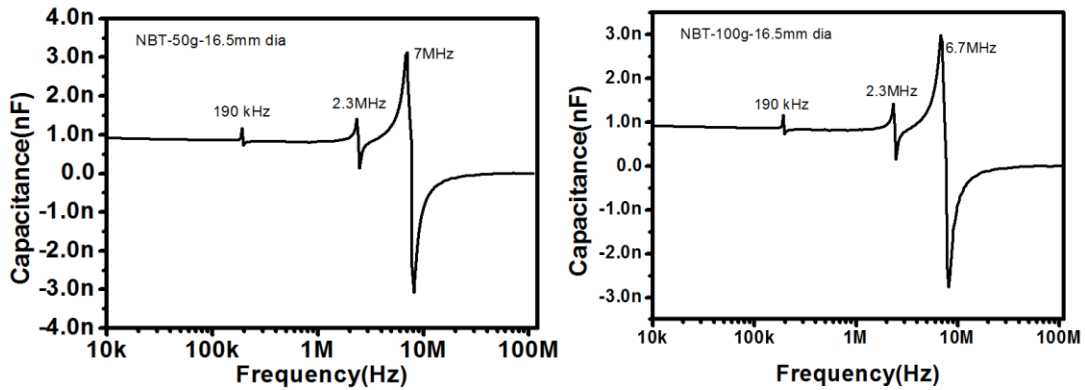

Fig 6.2: Piezoelectric resonance plots of NBT with 50 g and 100 g mass

After this we attached copper wires to the sample and metal base and those wires are connected to the BNC. This BNC is connected to the DSO (Digital storage oscilloscope). Now if we subject the NBT sample to vibrations, we can observe the change in the amplitude from the DSO.
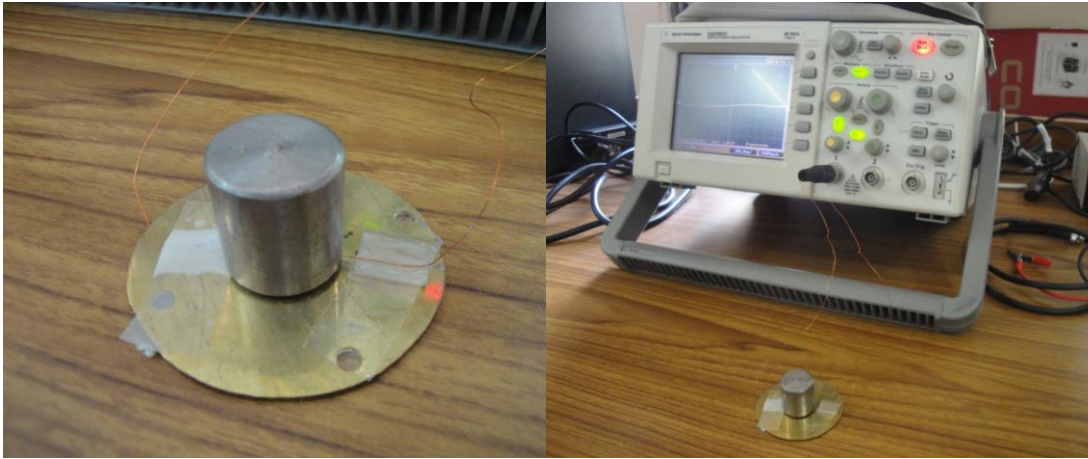
46

Fig 6.3: Experimental setup for testing the vibration sensor

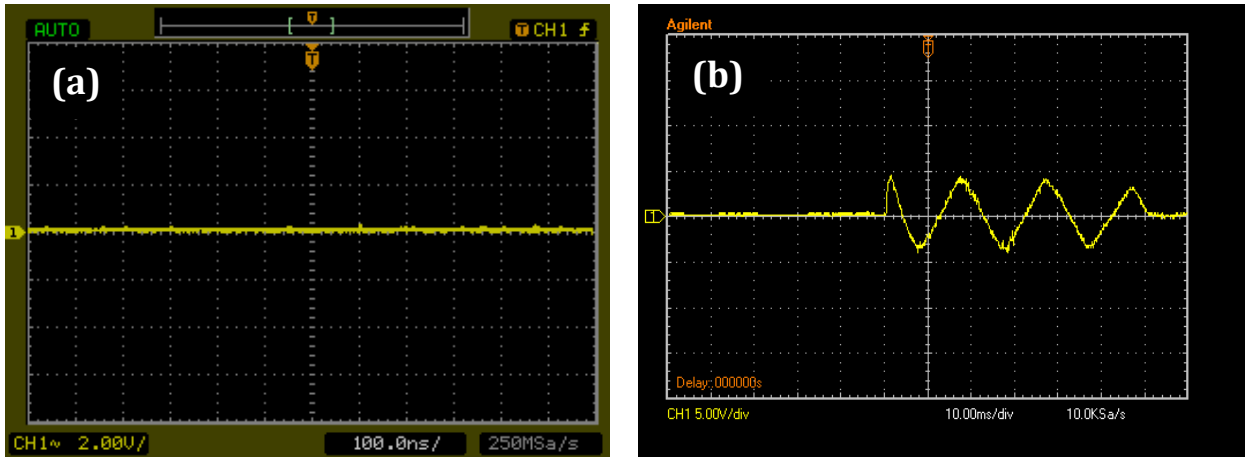The below figures shows the response of NBT to different vibrations.

Fig 6.4: Response of NBT (a) Without applying force (b) With applying force
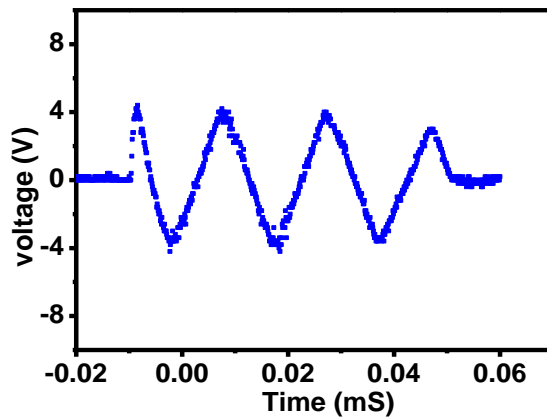
Fig 6.5: Response of NBT to applied force

47

The Fig. 6.4 (a) shows the response without applying any mass. After applying small force by tapping it, we observed the response from the material, and that was captured as Fig. 6.4 (b). Fig. 6.5 shows the response of the NBT to this force applied. Even though the response is less compared to PZT, NBT has the potential to be fabricated as a Sensor in lead free piezoelectric materials.

Chapter 7

Summary and Conclusions

7.1 Summary:

In this project work an attempt has been made to understand the relaxor features of NBT, Zr substituted NBT and NBT BT solid solution physical properties. These compositions were prepared by solid state route and analyzed the structural, morphological and physical properties with XRD, Raman spectroscopy, SEM, piezoelectric resonance and piezoelectric coefficient. At last NBT samples were tested for vibration sensor application.

7.2 Conclusions:

NBT with Zr substitution:

Phase pure NBT and NBZT5 were synthesized by solid state route where NBZT10 had some small impurity which is expected with higher Zr substitution.

1. Structural confirmations were done by XRD where there is no structural change in NBT by Zr substitution which was supported by Raman spectroscopy.

2. SEM analysis revealed the bismuth and sodium rich places with a platelet kind of structures in NBZT5 and NBZT10. Over all stoichiometry is as expected in NBT, NBZT5 and NBZt10 other that those plate like regions. The sample densities are also around 90% and there is increase in the grain size with Zr substitution.

3. Dielectric measurements revealed the decrease in the dielectric constant with increasing Zr concentration in NBT and there is no suppression in the AFE peak in Zr substituted NBT.

4. Piezoelectric resonance frequency measurements, piezoelectric coefficients (d_{33}) and electromechanically coupling coefficients (k_p) were decreased in NBZT (5, 10) compounds.

NBT–BT:

NBT – BT solid solution was prepared with two different compositions as NBT 6 BT (0.06 at % BT) and NBT8BT (0.08 at % BT). XRD revealed the phase purity of the compounds and indicated that there is no structural phase transition.

1. Scanning electron microscope images revealed that decrease in the grain size with increase in the BT concentration due to the less particle size of BT because it was synthesized by sol gel route. Overall composition followed proper stoichiometry.

2. Dielectric properties are changed in NBT – BT solid solution as T_d and T_m were decreased which is attributed to the increase in the piezo electric properties.

Vibration sensor study:

Vibration sensing capabilities of NBT were tested by using different vibrations. Results of the test proved the potential of NBT for vibration sensor applications.

Future work:

1. Synthesis of NBT-BT solid solution at MPB composition

2. Preparation of standard vibration sensor device with proper circuit.

3. Testing the vibration sensing abilities of NBT – BT compound.

References

1. Deborah D.L. Chung. Functional materials. World Scientific publishing Co. Pte. Ltd, 2010

2. Kawan Chi Kao. Dielectric phenomenon in solids. Elsevier Academic Press, 2004.

3. Matthew Delgado. Phase Transitions in Relaxor Ferroelectrics. (2005).

4. George A samara. The relaxational properties of compositionally disordered ABO_3 perovskites. Journal of Physics: Condensed Matter 15, (2003) R367-R411.

5. Water Heywang, Karl Lubitz and Wolfram Wersing. Piezoelectricity. Springer, 2008.

6. Charles Kittel. Introduction to Solid State Physics. 8th edition. John Wiley & Sons, Inc, 2005.

7. Abid A. shah. A FEM-BEM interactive coupling for modeling the piezoelectric health monitoring systems. Latin American Journal of solids and structures. 8, (2011) 305-334.

8. Uchino, Kenji. Advanced piezoelectric materials, Science and Technology. Woodhead publishing, Inc, 2010.

9. B K Barick, K K Mishra, A K Arora, R N P Choudhary and Dillip K Pradhan. Impedance and Raman spectroscopic studies of $(Na_{0.5}Bi_{0.5})$ TiO_3. Journal of Physics D: Applied Physics. 44, (2011) 355402.

10. M. Venkata Ramana, S. Roopas Kiran, N. Ramamanohar Reddy, K. V. Siva Kumar, V. R. K. Murthy, B. S. Murthy. Synthesis of lead free sodium bismuth titanate (NBT) ceramic by conventional and microwave sintering methods. Journal of Advanced Dielectrics 01, (2011) 71-77.

11. Giuseppe Viola, Huanpo Ning, Xiaojong Wei, Marco Deluca and Arturas Adomkevicius. Dielectric relaxation, lattice dynamics and polarization mechanisms in NBT. Journal of Applied Physics. 114, (2013) 014107.

12. Manish K Niranjan, T. Karthik, Saket Asthana, Jaysree Pan and Umesh V. Waghmare. Theoretical and experimental investigation of Raman modes, ferroelectric and dielectric properties of relaxor $Na_{0.5}Bi_{0.5}TiO_3$. Journal of Applied Physics. 113, (2013) 194106.

13. Elena Aksel, Jennifer S. Forrester, Humberto M. Foronda, Robert Dittmer and Dragan Damjanovic. Structure and properties of La-modified $Na_{0.5}Bi_{0.5}TiO_3$ at ambient and elevated temperatures. Journal of Applied Physics. 112, (2012) 054111.

14. Elena Aksel, Jennifer S. Forrester, Benjamin Kowalski, Marco Deluca, Dragan Damjanovic, and Jacob L. Jones. Structure and properties of Fe-modified $Na_{0.5}Bi_{0.5}TiO_3$ at ambient and elevated temperature. Physical Review B. 85, (2012) 024121.

15. Yeon Soo Sung and Myong Ho Kim. Effects of b site donor and acceptor doping in lead free $Bi_{0.5}Na_{0.5}TiO_3$ ceramics, Ferroelectrics. Chapter 13, In Tech, 2010.

16. Elena Aksel, and Jacob L. Jones. Advances in Lead-Free Piezoelectric Materials for Sensors and Actuators. Sensors 10, (2010) 1935-1954.

17. P.K. Panda. Environmental friendly lead free ceramics. Journal of Material Science. 44, (2009) 5049–5062.

18. Rohini Garg, Badari Narayana Rao, Anatoliy Senyshyn, P.S.R. Krishna and Rajeev Ranjan. Lead free piezoelectric system $(Na_{0.5}Bi_{0.5})TiO_3$-$BaTiO_3$: Equilibrium structures and irreversible structural phase transformations driven by electric field and mechanical impact. Physical Review B. 88, (2013) 014104.

19. Chenggang Xu, Dunmin Lin, and K.W. Wok. Structure, electrical properties and depolarization temperature of $(Bi_{0.5}Na_{0.5})TiO_3$-$BaTiO_3$ lead free piezoelectric ceramics. Solid state sciences, 10, (2008) 934-940.

20. Anthony R. WEST, Solid state chemistry and Its Applications. 2nd edition. John Wiley & Sons, Ltd, 2014.

21. G.S Upadhyaya. Powder Metallurgy Technology. Cambridge International Science Publishing, 2002.

22. Katsuyoshi Kondoh. Powder Metallurgy. In Tecch, 2012.

23. Zhigang Zak Fang. Sintering of Advanced Materials. Woodhead Publishing Limited, 2010.

24. Ted A Asare. Fabrication and damping behaviour of particulate $BaTiO_3$ ceramic reinforced copper matrix Composites. M.Sc Thesis. Virginia Polytechnic Institute and State University, Blacksburg, Virginia, 2004.

25. C. Jeffrey Brinker and George W. Scherer. Sol-Gel Science: The physics and chemistry of sol-gel processing. Academic Press. Inc, 1990.

26. B.D.Cullity. Elements of X-Ray Diffraction. Addison- Wesley Publishing Company, Inc, 1956.

27. J.D. Winefordner. Raman Spectroscopy for chemical analysis. John weily & Sons, Inc., 2000

28. Ray F. Egerton. Physical Principles of Electron Microscopy. Springer, 2005.

29. http://sensorwiki.org/doku.php/sensors/accelerometer

30. how sensors work - accelerometer - vibration sensors.htm

31. http://www.pcb.com/TechSupport/Tech_Accel

32. http://www.sensorsmag.com/sensors/acceleration-vibration/the-principles-piezoelectric-accelerometers-1022